compensate or to protect neurodegeneration induced by exposure to 500 ppm toluene.

In our previous study, we found a significant up-regulation of N-methyl D-aspartate (NMDA) receptor subunit NR2B expression associated with a simultaneous induction of CaMKIV, CREB1 and FosB/ΔFosB in the hippocampus of mice exposed to 50 ppm toluene for 12 weeks (Ahmed et al., 2007). In the present study, although the exposure to 50 ppm toluene for 6 weeks increased the expression of CREB1 mRNA in the hippocampus of mice, we did not observe any difference of CaMKIV expression. Therefore, activation of CREB-mediated gene transcription may require a prolonged period of exposure to toluene. Bale et al. (2005) suggested that the up-regulation of the functional expression of NMDA receptor subunits in the hippocampal neurons treated in vitro with toluene chronically, at human abusive level, as a compensatory response. Further study is needed to identify the hippocampus-specific upstream regulators or downstream targets of CREB that serve as Ca^{2+} dependent kinases. To the best of our knowledge, only a few studies have examined the effects of long-term toluene exposure on the expression of dopamine receptors in adult mouse hippocampus. Dopamine D1/D5 receptors have a novel neuromodulatory role in regulating hippocampal synaptic plasticity, i.e., time-dependent reversal of NMDAR-dependent long-term depression (Mockett et al., 2007). Recently, it has been reported that ciliary neurotrophic factor mediates dopaminergic innervations and D2 receptor-induced neurogenesis in the adult brain (Yang et al., 2008). However, a link between NGF and dopaminergic system is not clear. Therefore, we also examined the dopamine receptors D1, D2 and related enzyme TH gene expressions in this study. However, we did not observe any significant difference between treatment groups. One of the possibilities is NGF mediates different mechanism to induce neurogenesis in the hippocampus independent of dopaminergic system in the mouse hippocampus.

Although many epidemiological studies have demonstrated the causative factors, susceptible populations and clinical implications for multiple chemical sensitivity (MCS) (Graveling et al., 1999; Ross et al., 1999; Bolt and Kiesswetter, 2002), the pathophysiology of the disease is still unclear. It is assumed that the affected individuals react to widely different types of chemical stimuli in very low concentrations that would not cause any reaction in the general population (Cullen, 1987). However, genetic factors may play a role in the etiology of MCS and analysis of genetic factors becomes possible and new approaches to identify the mechanism of MCS.

An increased NGF level was occurred in plasma of MCS patients (Kimata, 2004). Then, the MCS patients showed significantly higher capsaicin cough sensitivity than the healthy controls, supporting a hypothesis that NGF-related neurogenic mechanisms are involved in MCS (Ternesten-Hasseus et al., 2002). Our results indicate that low-level toluene exposure may induce up-regulation of neurotrophin-related gene expression in the mouse hippocampus depending on the mouse strain and an allergic stimulation in sensitive strain may decrease the threshold for sensitivity at lower exposure level.

In conclusion, this is the first study to demonstrate that exposure to low levels of toluene up-regulated the expression of neurotrophins and their receptors in adult mouse hippocampus in a strain-dependent manner and in accordance with the allergic condition. Further studies are needed to evaluate the existence of a positive relation between NGF–TrkA-signal transduction pathway and neurobehavioral alterations following toluene exposure.

Conflict of interest statement

We have no conflicting interests to declare.

Acknowledgments

This research was partly supported by a grant from the Ministry of Education, Culture, Sports, Sciences and Technology, Japan (#18390189, #21390198) to H.F. We thank Ms. K. Ohnishi and K. Taki for their technical assistance.

References

Ahmed S, Win-Shwe TT, Yamamoto S, Tsukahara S, Kunugita N, Arashidani K, Fujimaki H. Increased hippocampal mRNA expression of neuronal synaptic plasticity related genes in mice chronically exposed to toluene at a low-level human occupational-exposure. Neurotoxicology 2007;28:168–74.
Allen SJ, Dawbarn D. Clinical relevance of the neurotrophins and their receptors. Clin Sci (Lond) 2006;110:175–91.
Aloe L, Alleva E, Fiore M. Stress and nerve growth factor: findings in animal models and humans. Pharmacol Biochem Behav 2002;73:159–66.
American Conference of Governmental Industrial Hygienists (ACGIH). Threshold limit values and biological exposure indices guide; 2006. www.acgih.org/TLV/Studies.htm.
Bale AS, Tu Y, Carpenter-Hyland EP, Chandler LJ, Woodward JJ. Alterations in glutamatergic and GABAergic ion channel activity in hippocampal neurons following exposure to the abused inhalant toluene. Neuroscience 2005;130:197–206.
Barde YA. Neurotrophins: a family of proteins supporting the survival of neurons. Prog Clin Biol Res 1994;390:45–56.
Bedogni B, Pani G, Colavitti R, Riccio A, Borrello S, Murphy M, Smith R, Eboli ML, Galeotti T. Redox regulation of cAMP-responsive element-binding protein and induction of manganous superoxide dismutase in nerve growth factor-dependent cell survival. J Biol Chem 2003;278:16510–9.
Benignus VA, Boyes WK, Bushnell PJ. A dosimetric analysis of behavioral effects of acute toluene exposure in rats and humans. Toxicol Sci 1998;43:186–95.
Betancourt AM, Burgess SC, Carr RL. Effect of developmental exposure to chlorpyrifos on the expression of neurotrophin growth factors and cell-specific markers in neonatal rat brain. Toxicol Sci 2006;92:500–6.
Bolt HM, Kiesswetter E. Is multiple chemical sensitivity a clinically defined entity? Toxicol Lett 2002;128:99–106.
Bonini S, Lambiase A, Bonini S, Angelucci F, Magrini L, Manni L, Aloe L. Circulating nerve growth factor levels are increased in humans with allergic diseases and asthma. Proc Natl Acad Sci U S A 1996;93:10955–60.
Bowen SE, McDonald P. Abuse pattern of toluene exposure alters mouse behavior in a waiting-for-reward operant task. Neurotoxicol Teratol 2009;31:18–25.
Brown RE, Wong AA. The influence of visual ability on learning and memory performance in 13 strains of mice. Learn Mem 2007;14:134–44.
Chao MV, Rajagopal R, Lee FS. Neurotrophin signalling in health and disease. Clin Sci (Lond) 2006;110:167–73.
Cullen MR. The worker with multiple chemical sensitivities: an overview. Occup Med 1987;2:655–61.
Fujimaki H, Kurokawa Y, Kunugita N, Kikuchi M, Sato F, Arashidani K. Differential immunogenic and neurogenic inflammatory responses in an allergic mouse model exposed to low levels of formaldehyde. Toxicology 2004;197:1–13.
Fujimaki H, Yamamoto S, Win-Shwe TT, Hojo R, Sato F, Kunugita N, Arashidani K. Effect of long-term exposure to low-level toluene on airway inflammatory response in mice. Toxicol Lett 2007;168:132–9.
Gelazonia L, Japaridze N, Svanidze I. Pyramidal cell loss in hippocampus of young rats exposed to toluene. Georg Med News 2006;135:126–8.
Goddard CA, Butts DA, Shatz CJ. Regulation of CNS synapses by neuronal MHC class I. Proc Natl Acad Sci U S A 2007;104:6828–33.
Graveling RA, Pilkington A, George JP, Butler MP, Tannahill SN. A review of multiple chemical sensitivity. Occup Environ Med 1999;56:73–85.
Hori H, Ishidao T, Oyabu T, Yamato H, Morimoto Y, Tanaka I. Effect of simultaneous exposure to methanol and toluene vapor on their metabolites in rats. J Occup Health 1999;41:149–53.
Huh GS, Boulanger LM, Du H, Riquelme PA, Brotz TM, Shatz CJ. Functional requirement for class I MHC in CNS development and plasticity. Science 2000;290:2155–9.
Japan Society for Occupational Health. Toluene. Ind Med 1994;36:103–10.
Kamath AB, Alt J, Debbabi H, Taylor C, Behar SM. The major histocompatability complex haplotype affects T-cell recognition of Mycobacterial antigens but not resistance to *Mycobacterium tuberculosis* in C3H mice. Infect Immun 2004;72:6790–8.
Kidd SK, Anderson DW, Schneider JS. Postnatal lead exposure alters expression of forebrain p75 and TrkA nerve growth factor receptors. Brain Res 2008;1195:113–9.
Kimata H. Effect of exposure to volatile organic compounds on plasma levels of neuropeptides, nerve growth factor and histamine in patients with self-reported multiple chemical sensitivity. Int J Hyg Environ Health 2004;207(2):159–63.
Korbo L, Ladefoged O, Lam HR, Ostergaard G, West MJ, Arlien-Søborg P. Neuronal loss in hippocampus in rats exposed to toluene. Neurotoxicology 1996;17:359–66.
Levi-Montalcini R, Aloe L, Alleva E. A role for nerve growth factor in nervous, endocrine and immune systems. Prog Neurol Endocrinol Immunol 1990;3:1–10.
Lindsay RM, Harmar AJ. Nerve growth factor regulates expression of neuropeptide genes in adult sensory neurons. Nature 1989;337:362–4.
Lindvall O, Ernfors P, Bengzon J, Kokaia Z, Smith ML, Siesjö BK, Persson H. Differential regulation of mRNAs for nerve growth factor, brain-derived neurotrophic factor, and neurotrophin 3 in the adult rat brain following cerebral ischemia and hypoglycemic coma. Proc Natl Acad Sci U S A 1992;89:648–52.

Mockett BG, Guévremont D, Williams JM, Abraham WC. Dopamine D1/D5 receptor activation reverses NMDA receptor-dependent long-term depression in rat hippocampus. J Neurosci 2007;27:2918–26.
Nakajima D, Tin-Tin-Win-Shwe, Kakeyama M, Fujimaki H, Goto S. Determination of toluene in brain of freely moving mice using solid-phase microextraction technique. Neurotoxicology 2006;27:615–8.
Nockher WA, Renz H. Neurotrophins in allergic diseases: from neuronal growth factors to intercellular signaling molecules. J Allergy Clin Immunol 2006;117:583–9.
Okuyama K, Ohwada K, Sakurada S, Sato N, Sora I, Tamura G, Takayanagi M, Ohno I. The distinctive effects of acute and chronic psychological stress on airway inflammation in a murine model of allergic asthma. Allergol Int 2007;56:29–35.
Ross PM, Whysner J, Covello VT, Kuschner M, Rifkind AB, Sedler MJ, Trichopoulos D, Williams GM. Olfaction and symptoms in the multiple chemical sensitivities syndrome. Prev Med 1999;28:467–80.
Sanico AM, Koliatsos VE, Stanisz AM, Bienenstock J, Togias A. Neural hyperresponsiveness and nerve growth factor in allergic rhinitis. Int Arch Allergy Immunol 1999;118:154–8.
Sari DK, Kuwahara S, Tsukamoto Y, Hori H, Kunugita N, Arashidani K, Fujimaki H, Sasaki F. Effects of prolonged exposure to low concentrations of formaldehyde on the corticotrophin releasing hormone neurons in the hypothalamus and adrenocorticotropic hormone cells in the pituitary gland in female mice. Brain Res 2004;1013:107–16.
Sari DK, Kuwahara S, Tsukamoto Y, Hori H, Kunugita N, Arashidani K, Fujimaki H, Sasaki F. Effect of subchronic exposure to low concentrations of toluene on the hypothalamo-pituitary adrenal gland axis of female mice. J Jpn Soc Atmos Environ 2006;42:38–43.
Terashi H, Nagata K, Satoh Y, Hirata Y, Hatazawa J. Hippocampal hypoperfusion underlying dementia due to chronic toluene intoxication. Rinsho Shinkeigaku 1997;37:1010–3.
Ternesten-Hasseus E, Bende M, Millqvist E. Increased capsaicin cough sensitivity in patients with multiple chemical sensitivity. J Occup Environ Med 2002;44:1012–7.
United States Environmental Protection Agency. Prepared by the Office of Pollution Prevention and Toxics. Chemicals summary of toluene, EPA; 1994: 749-F-94-021a.
von Euler G, Ogren SO, Li XM, Fuxe K, Gustafsson JA. Persistent effects of subchronic toluene exposure on spatial learning and memory, dopamine-mediated locomotor activity and dopamine D2 agonist binding in the rat. Toxicology 1993;77:223–32.
von Euler M, Pham TM, Hillefors M, Bjelke B, Henriksson B, von Euler G. Inhalation of low concentrations of toluene induces persistent effects on a learning retention task, beam-walk performance, and cerebrocortical size in the rat. Exp Neurol 2000;163:1–8.
Win-Shwe TT, Mitsushima D, Nakajima D, Ahmed S, Yamamoto S, Tsukahara S, Kakeyama M, Goto S, Fujimaki H. Toluene induces rapid and reversible rise of hippocampal glutamate and taurine neurotransmitter levels in mice. Toxicol Lett 2007a;168:75–82.
Win-Shwe TT, Yamamoto S, Nakajima D, Furuyama A, Fukushima A, Ahmed S, Goto S, Fujimaki H. Modulation of neurological related allergic reaction in mice exposed to low-level toluene. Toxicol Appl Pharmacol 2007b;222:17–24.
Win-Shwe TT, Mitsushima D, Yamamoto S, Funabashi T, Fujimaki H. Strain differences in extracellular amino acid neurotransmitter levels in the hippocampi of major histocompatibility complex congenic mice in response to toluene exposure. Neuroimmunomodulation 2009;16:185–90.
Win-Shwe TT, Kunugita N, Yamamoto S, Arashidani K, Fujimaki H. Strain differences influence NMDA receptor subunit gene expression in olfactory bulb of an allergic mouse model following toluene exposure. Neuroimmunomodulation; in press.
Yan C, Liang Y, Nylander KD, Schor NF. TrkA as a life and death receptor: receptor dose as a mediator of function. Cancer Res 2002;62:4867–75.
Yang P, Arnold SA, Habas A, Hetman M, Hagg T. Ciliary neurotrophic factor mediates dopamine D2 receptor-induced CNS neurogenesis in adult mice. J Neurosci 2008;28:5867–9.

Contents lists available at ScienceDirect

Toxicology in Vitro

journal homepage: www.elsevier.com/locate/toxinvit

Use of live imaging analysis for evaluation of cytotoxic chemicals that induce apoptotic cell death

Yoshiko Koike-Kuroda [a], Masaki Kakeyama [b,c], Hidekazu Fujimaki [c], Shinji Tsukahara [a,c,*]

[a] Department of Regulation Biology, Graduate School of Science and Engineering, Saitama University, Shimo-Okubo 255, Sakura-ku, Saitama City, Saitama 338-8570, Japan
[b] Laboratory of Environmental Health Sciences, Graduate School of Medicine, Center for Disease Biology and Integrative Medicine, The University of Tokyo, Hongo 7-3-1, Bunkyo-ku, Tokyo 113-0033, Japan
[c] Research Center for Environmental Risk, National Institute for Environmental Studies, Onogawa 16-2, Tsukuba, Ibaraki 305-8506, Japan

ARTICLE INFO

Article history:
Received 3 March 2010
Accepted 27 July 2010
Available online 1 August 2010

Keywords:
Caspase-3
Apoptosis
Live imaging
Sodium arsenite

ABSTRACT

We carried out live imaging of PC12 cells expressing SCAT3, a caspase-3 cleavage peptide sequence linking two fluorescent proteins, ECFP and Venus, which function respectively as the donor and acceptor for FRET. Live imaging of SCAT3-expressing cells was performed from 60 to 300 min after exposure to sodium arsenite ($NaAsO_2$: 0, 1, 5, or 10 μM) was initiated. We then measured the emission ratio of ECFP to Venus to monitor the activity of caspase-3 and found that the ratio was temporally and dose-dependently increased by $NaAsO_2$. The mean ECFP/Venus emission ratio between 200 and 300 min after exposure to $NaAsO_2$ at a dose of 5 or 10 μM, but not at 1 μM, was significantly higher than that in the control group. We showed by other methods that $NaAsO_2$ significantly increased the amount and activity of mature caspase-3 and the amount of nucleosomes generated from DNA fragmentation, and decreased cell viability. However, methods other than live imaging required a longer time and higher doses of $NaAsO_2$ than did live imaging to detect significant effects. This result suggests that live imaging using SCAT3 is a useful method for the screening of chemical toxicities and for improving the efficiency of toxicity evaluation.

1. Introduction

Apoptosis is a phenomenon that controls cell fate and determines cell survival and cell death. Cell death by apoptosis often, although not always, occurs if the cells are exposed to toxic chemicals. Heavy metal compounds, which are capable of causing numerous acute or chronic pathologies, are known to induce apoptotic cell death (Rana, 2008). For example, the inorganic arsenic compounds, sodium arsenite ($NaAsO_2$) and arsenic trioxide, exhibit cytotoxicity accompanied by the induction of apoptotic cell death in a variety of cells, including immune cells (Bustamante et al., 1997; Hossain et al., 2000), neuronal cells (Namgung and Xia, 2001; Wong et al., 2005; Chattopadhyay et al., 2002), a gastric cancer cell line (Jiang et al., 2001), a leukemia cell line (Iwama et al., 2001), and a neuroblastoma cell line (Watcharasit et al., 2008). In addition, cell death by apoptosis occurs when cells are exposed to other heavy metal compounds, such as lead acetate (Shabani and Rabbani, 2000; Columbano et al., 1985), lead nitrate (Pachauri et al., 2009), hexavalent chromium (Hill et al., 2008; Carlisle et al., 2000; Wang et al., 2000; Azad et al., 2008; Gambelunghe et al., 2006; Rudolf and Cervinka, 2006), methyl mercury (Homma-Takeda et al., 2001; Close et al., 1999; Shenker et al., 1999; Toimela and Tahti, 2004), mercuric chloride (Araragi et al., 2003), and cadmium chloride (Dong et al., 2001; Choi et al., 2002; Gennari et al., 2003; Habeebu et al., 1998). Caspase-3 is an executor proteinase of apoptosis, whose enzymatic activity is stimulated by death signals. It has been reported that the caspase-3 of cells cultured *in vitro* is activated by lead acetate (Dong et al., 2009), hexavalent chromium (Hill et al., 2008; Russo et al., 2005), methyl mercury (Toimela and Tahti, 2004), arsenic trioxide (Jiang et al., 2001; Tse et al., 2008, 2009; Piga et al., 2007) or $NaAsO_2$ (Watcharasit et al., 2008). The combined data suggest that activation of caspase-3 may be a major irreversible step towards apoptotic cell death following exposure to such heavy metal compounds. Thus, the activity of caspase-3 is a suitable end-point for evaluation of the cytotoxicity of chemicals.

Abbreviations: ECFP, enhanced cyan fluorescent protein; FRET, fluorescence resonance energy transfer; $NaAsO_2$, sodium arsenite; NGF, nerve growth factor; PBS, phosphate-buffered saline; PEI, polyethyleneimine; pNA, *p*-nitroanilide; SDS, sodium dodecyl sulfate; Z-VAD-FMK, *N*-benzyloxycarbonyl-Val-Ala-Asp-fluoromethylketone (broad-spectrum caspase inhibitor).

* Corresponding author at: Department of Regulation Biology, Graduate School of Science and Engineering, Saitama University, Shimo-Okubo 255, Sakura-ku, Saitama City, Saitama 338-8570, Japan. Tel./fax: +81 48 858 3420.
E-mail address: stsuka@mail.saitama-u.ac.jp (S. Tsukahara).

0887-2333/$ - see front matter © 2010 Elsevier Ltd. All rights reserved.
doi:10.1016/j.tiv.2010.07.022

The dynamics and temporal patterns of caspase activation can be monitored by fluorescence resonance energy transfer (FRET) methods. In a single living cell undergoing apoptosis, temporal changes in the activity of caspase-3 are profiled by measurement of the extent of FRET within a recombinant substrate composed of enhanced cyan fluorescent protein (ECFP) linked by the caspase-3 cleavage sequence, Asp-Glu-Val-Asp (DEVD), to enhanced yellow fluorescent protein (EYFP) (Tyas et al., 2000; Luo et al., 2001; Rehm et al., 2002). In addition, Takemoto et al. improved such a recombinant substrate by replacing EYFP with a variant of EFYP named Venus (Nagai et al., 2002) and called the improved indicator for caspase-3 activation "SCAT3" (Takemoto et al., 2003). The usefulness of FRET technology using SCAT3 for monitoring caspase-3 activation in living cells both *in vitro* and *in vivo* has been well documented (Takemoto et al., 2003; Kanuka et al., 2005; Kuranaga et al., 2006; Takemoto et al., 2007).

In the present study, we applied live cell imaging analysis using SCAT3 for determination of cytotoxic effects of chemicals on the PC12 cell line, which is a cell line derived from a pheochromocytoma of rat adrenal medulla and which has the potential to differentiate into neuron-like cells. By live imaging of SCAT3-expressing PC12 cells, we profiled the temporal changes in caspase-3 activity after exposure of the cells to $NaAsO_2$. In addition, we examined the effects of $NaAsO_2$ on apoptosis induced by other methods to determine whether the sensitivity and efficiency of detection of toxicity is improved by live imaging analysis using SCAT3. In this study, we performed western blotting analysis for determination of the protein expression of the cleaved, active form of caspase-3, measured the enzymatic activity of caspase-3, the amount of nucleosomes generated from apoptotic DNA fragmentation, and the viability of PC12 cells after they were exposed to $NaAsO_2$.

2. Materials and methods

2.1. Cell culture and reagent preparation

PC12 cells (Collection No. IFO50278; the Health Science Research Resources Bank, Kobe, Japan) were used to test the usefulness of the SCAT3 system for detection of $NaAsO_2$ toxicity. The effects of $NaAsO_2$ on the protein expression and enzymatic activity of caspase-3, on DNA fragmentation, and on cell viability were assayed. PC12 cells were maintained in RPMI 1640 medium (Gibco-Invitrogen, Carlsbad, CA, USA) containing 10% horse serum, 5% fetal bovine serum, 0.1 mM Non-Essential Amino Acids Solution (Invitrogen, Carlsbad, CA, USA), a mixture of penicillin and streptomycin (100 units/ml and 100 μg/ml each; Invitrogen), and 100 μg/ml normocin (InvivoGen, San Diego, CA, USA) in 75-cm^2 flasks coated with poly-D-lysine (Becton Dickinson and Co., Oxford, UK) in an atmosphere containing 5% CO_2 at 37 °C. PC12 cells at passage 7–12 were used for the following experiments.

For each experiment, PC12 cells were cultured in medium that was exclusively used for experiments and not for cell maintenance. This medium hereafter referred to as experimental medium consisted of RPMI 1640 medium (Gibco-Invitrogen) containing 0.01 mM Non-Essential Amino Acids Solution (Invitrogen), a mixture of penicillin and streptomycin (10 units/ml and 10 μg/ml each; Invitrogen) and 10 μg/ml normocin (InvivoGen), with or without supplementation with 1% horse serum and 0.5% fetal bovine serum. PC12 cells cultured in this medium were simultaneously treated with nerve growth factor (NGF; 50 ng/ml) for neuron-like cell differentiation and were exposed to $NaAsO_2$ (Wako Pure Chemical Industries, Osaka, Japan) at a dose of 0, 1, 5, or 10 μM. Crystalline $NaAsO_2$ was dissolved in sterile-filtered water (Sigma–Aldrich, St. Louis, MO, USA) at a concentration of 100 mM. $NaAsO_2$ solution (100 mM) was diluted with experimental medium with or without serum supplementation to generate the indicated concentrations.

2.2. Transfection and imaging analysis of SCAT3

PC12 cells (10^6 cells) were transfected with 2.0 μg of the SCAT3 expression vector pcDNA-SCAT3, provided by Dr. M. Miura (University of Tokyo, Tokyo, Japan) (Takemoto et al., 2003), using Nucleofector™ II (Lonza Cologne AG, Cologne, Germany). PC12 cells (10^4 cells/well) were then seeded onto 8-well chamber slides (LAB-TEK™ Chambered Coverglass; Nalge Nunc International, Rochester, NY, USA) coated with 0.25% polyethyleneimine (PEI; Sigma–Aldrich) and were cultured in the above-described subculture medium (300 μl) under an atmosphere containing 5% CO_2 at 37 °C.

One or two days after transfection, live imaging of SCAT3-expressing PC12 cells was performed using a fluorescent time-lapse microscope BioZero 8100 (Keyence Co., Osaka, Japan) controlled by a computer with a BZ Viewer version 1.0 software installed (Keyence). SCAT3-expressing PC12 cells were simultaneously treated with NGF (50 ng/ml) and exposed to $NaAsO_2$ (0 or 10 μM) in 300 μl of experimental medium with or without serum supplementation. Live imaging of such cells was then carried out in five independent experiments. In some experiments, SCAT3-expressing PC12 cells were simultaneously treated with NGF (50 ng/ml) and exposed to $NaAsO_2$ at a dose of 0, 1, 5, or 10 μM in serum supplemented experimental medium. Live imaging of these cells was then performed in five independent experiments.

SCAT3-expressing PC12 cells were placed in an incubation chamber (Microscope Incubation System INU-KI-F1, Tokai Hit, Shizuoka, Japan) whose temperature was controlled at 37 °C and within which the gas concentration was maintained at 5% CO_2 and 95% air. Fluorescent time-lapse imaging was started at 60 min and ended at 300 min after initiation of $NaAsO_2$ exposure. A 440AF21 excitation filter, a 455DRLP dichroic mirror, and two emission filters 480AF30 for ECFP and 535AF25 for Venus (Opto Science Inc., Tokyo, Japan) were used for imaging of SCAT3-expressing cells. The excitation intensity was attenuated to 40% of the maximum power of a light source with a neutral density filter. Fluorescent images of SCAT3 were captured every 20 min using an objective lens (Plan Fluor ELWD DM 20xC, NA 0.45; Nikon, Tokyo, Japan) and a CCD camera in the KEYENCE BioZero 8100.

After live imaging was completed for each experiment, the intensity of ECFP and Venus emissions of SCAT3-expressing PC12 cells was measured using the digital image data. The region of interest corresponded to from 1.12 to 1.69 mm of the cultured slides (the mean number of SCAT3-expressing PC12 cells: approx. 150). The RGB digital images of ECFP (*cyan blue*) and Venus (*yellow green*) taken from SCAT3-expressing PC12 cells were converted into monochromatic color images (*red* for ECFP; *green* for Venus). These images were merged at each time point in order to determine the intensities of ECFP and Venus of the same region, which were obtained by measuring the brightness of *red* and *green* colors, respectively with the aid of a computer and the KEYENCE BZ Viewer version 1.0 software (Keyence). After the brightness values of *red* and *green* colors in the same region of each merged image were measured, the ECFP/Venus emission ratio was calculated by dividing the brightness value of the *red* color by that of the *green* color. The ECFP/Venus emission ratio at each time point was calibrated using the ratio of the same area at 60 min after $NaAsO_2$ exposure, which was set at a value of 1.

2.3. Western blot analysis of caspase-3

PC12 cells, seeded on 0.25% PEI-coated 12-well plates, (10^5 cells/well) were treated with NGF (50 ng/ml) and exposed to

$NaAsO_2$ (0, 1, 5, or 10 μM) in 1 ml of serum supplemented experimental medium. These cells were rinsed in phosphate-buffered saline (PBS) 360 and 1200 min after exposure to $NaAsO_2$, and were then collected in PBS containing a protease inhibitor cocktail (EDTA-free Complete Mini; Roche Diagnostics, Basel, Switzerland) on ice. After the cells were centrifuged at 1500 rpm for 10 min at 4 °C, the cell pellets were homogenized in lysis buffer (CelLytic; Sigma–Aldrich) containing a protease inhibitor cocktail (1:4000; Sigma–Aldrich). PC12 cells, exposed to $NaAsO_2$ at different doses, were collected from five and four independent experiments for 360-min and 1200-min exposure, respectively.

The cell lysate of each sample was mixed with 1/4 volume of 0.29 M Tris–Hcl (pH 6.8) containing 8.3% sodium dodecyl sulfate (SDS), 25% glycerol, 7.75% dithiothreitol, and 0.01% bromphenol blue, and was then boiled at 95 °C for 4 min. Equal amounts of protein (5 μg) were resolved by electrophoresis on 15% SDS–polyacrylamide gels, and the proteins were transferred to PVDF membranes by semidry transfer using an iBlot module (Invitrogen). After transfer, the membranes were rinsed in TBST (20 mM Tris–HCl containing 0.9% NaCl, and 0.1% Tween-20, pH 7.6) and were treated with a blocking buffer (Blocking One; Nakalai Tesque, Inc., Kyoto, Japan) for 1 h at room temperature. The membranes were incubated with a rabbit anti-caspase-3 antibody (1:2000; Cell Signaling Technology, Beverly, MA, USA), which can detect both cleaved caspase-3 (an active caspase-3) and non-cleaved caspase-3 (procaspase-3), at 4 °C overnight before and after rinsing in TBST. Membranes were successively incubated with horseradish peroxidase-conjugated goat anti-rabbit IgG (1:2000, Cell Signaling) in TBST for 1 h at room temperature. Immunoreactive signals for specific proteins were visualized on an X-ray film using a chemiluminescence reagent.

The levels of immunoreactive signals for caspase-3 were determined using ImageJ 1.31 software (National Institutes of Health, Bethesda, MD, USA). The level of cleaved caspase-3 was normalized by dividing by the total amount of caspase-3 in the same lane of the blotting membrane. The percent of cleaved caspase-3 in total caspase-3 was expressed relative to controls (0 μM of $NaAsO_2$) that were set at 100% for each experiment.

2.4. Caspase-3 activity assay

PC12 cells were cultivated in 0.25% PEI-coated 6-well plates up to 80–90% confluency, and were then treated with NGF (50 ng/ml) and exposed to $NaAsO_2$ (0, 1, 5 or 10 μM) for 360 or 1200 min in 2 ml of serum supplemented experimental medium In addition, some of PC12 cells were exposed to 10 μM of $NaAsO_2$ and were treated with 50 μM of *N*-benzyloxycarbonyl-Val-Ala-Asp-fluoromethylketone (Z-VAD-FMK), a broad-spectrum caspase inhibitor (Promega, Madison, WI, USA) for 1200 min. PC12 cell in each group were collected from four or five independent experiments.

After protein was extracted from the collected cells, an equal amount of total protein (35 μg) from each sample was used for the measurement of caspase-3 activity. The activity of caspase-3 in cell extracts was evaluated by assessing cleavage of the colorimetric substrate, a DEVD peptide-conjugated with *p*-nitroanilide (pNA), using a caspase-3 activity assay kit (CaspACE™ assay system, Colorimetric; Promega) in accordance with the manufacturer's protocol. The activity of caspase-3 was expressed as the amount of free pNA per unit protein (pmol/μg).

2.5. Apoptosis assay

PC12 cells, seeded on 0.25% PEI-coated 96-well plates (10^4 cells/well), were treated with NGF (50 ng/ml) and exposed to $NaAsO_2$ at a dose of 0, 1, 5 or 10 μM for 1200 min in 100 μl of serum supplemented experimental medium. The effect of $NaAsO_2$ on DNA fragmentation was examined using a Cell Death Detection ELISA Plus Assay kit (Roche Diagnostics) in accordance with the manufacturer's protocol. This assay was performed using four independent experiments. The amount of nucleosomes generated from DNA fragmentation was expressed relative to that of controls (0 μM of $NaAsO_2$) that were set at 100% for each experiment.

2.6. Cell viability assay

The effects of $NaAsO_2$ on the viability of PC12 cells were determined in six independent experiments using a colorimetric assay based on the reduction of tetrazolium salt to formazan by mitochondrial dehydrogenase activity. PC12 cells, seeded on 0.25% PEI-coated 96-well plates (10^4 cells/well), were treated with NGF (50 ng/ml) and exposed to $NaAsO_2$ (0, 1, 5 or 10 μM) in triplicate for 1 or 2 days in 100 μl of serum supplemented experimental medium. Ten microliters of Tetrazolium reagent WST-1 (Roche Applied Bioscience, Indianapolis, IN, USA) was then reacted with the cells for 1–3 h at 37 °C, and absorbance at 450 nm was then measured using a reference wavelength of 650 nm. The absorbance at 650 nm was subtracted from the absorbance at 450 nm, and this value was then expressed as a percentage of the value obtained for PC12 cells without $NaAsO_2$ exposure, whose viability was set at 100%.

2.7. Statistical analyses

Overall differences in the temporal changes in the ECFP/Venus emission ratio among groups were analyzed using two-way factorial analysis of variance (ANOVA) for repeated measures. When significant overall effects were detected contrast analyses between groups were then performed. The overall effects of culture conditions and $NaAsO_2$ on the mean of the ECFP/Venus emission ratio were examined using two-way ANOVA. One-way ANOVA was performed to determine differences among groups with respect to the mean of the ECFP/Venus emission ratio, the amount of cleaved caspase-3, the activity of caspase-3, the amount of apoptotic nucleosomes, and cell viability. When significant overall effects were detected by two-way or one-way ANOVA, Fisher's PLSD test was performed for post hoc analysis.

3. Results

3.1. Effects of serum supplementation and $NaAsO_2$ exposure on SCAT3-expressing cells

We first assayed the FRET signal of the caspase-3 cleavage FRET reporter SCAT3, following exposure of SCAT3-expressing PC12 cells to $NaAsO_2$ in the presence or absence of serum. The fluorescence intensities of Venus (*yellow green*) and ECFP (*cyan blue*), and the morphology of SCAT3-expressing PC12 cells, were altered over time by $NaAsO_2$ exposure under all culture conditions (Fig. 1A and C). The ratio of ECFP to Venus emissions was calculated by dividing the brightness value of the *red* signal (ECFP) by that of the *green* signal (Venus), after the images of ECFP and Venus were converted into monochromatic images (ECFP: *cyan blue* to *red*; Venus: *yellow green* to *green*).

This ratio increased as the time of exposure to 10 μM of $NaAsO_2$ under serum-free culture conditions was increased, and peaked at 220–240 min (Fig. 1B). However, under these serum-free culture conditions, the temporal pattern of the ECFP/Venus emission ratio did not significantly [$F(12, 96) = 1.52$, $p = 0.13$] differ between the control and the $NaAsO_2$-exposed groups. This result was due to the fact that there was a gradual increase in this ratio over time even in the control group under serum-free culture conditions.

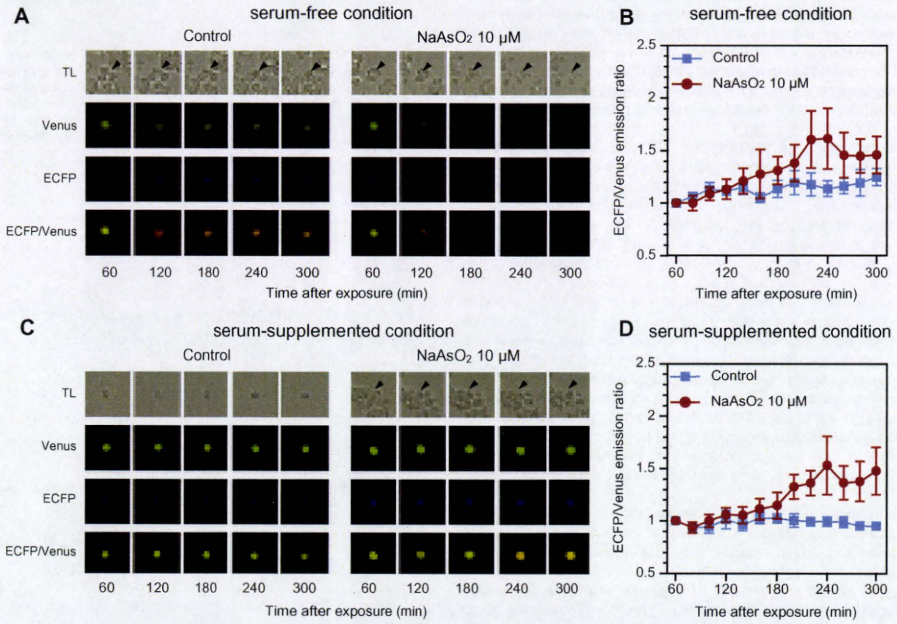

Fig. 1. Effects of culture serum conditions on SCAT3-expressing PC12 cells during exposure to $NaAsO_2$. Imaging analyses of SCAT3-expressing PC12 cells during exposure to $NaAsO_2$ (0 or 10 μM) were performed under serum-free culture conditions (A and B) or serum-supplemented culture conditions (C and D). A and C: Time-lapse images of SCAT3-expressing PC12 cells captured with transmitted light (TL), emissions of ECFP (*cyan blue*) and Venus (*yellow green*), and merged images of Venus and ECFP after conversion of fluorescent colors into pseudo colors (ECFP: *cyan blue* to *red*; Venus: *yellow green* to *green*) arrowheads indicate SCAT3-expressing cells. B and D: temporal changes in the emission ratio of ECFP to Venus of SCAT3-expressing cells. The ratio at each time point was calibrated using the ratio at 60 min after exposure, which was set at 1. Values are the means ± SEM of five independent experiments. (For interpretation of the references to color in this figure legend, the reader is referred to the web version of this article.)

Under serum-supplemented culture conditions, the ECFP/Venus emission ratio began to increase at 180 min, and peaked at 240 min after SCAT3-expressing PC12 cells were exposed to 10 μM of $NaAsO_2$ (Fig. 1D). In contrast, in the control group under serum-supplemented culture conditions, the ECFP/Venus emission ratio did not change over time and was maintained at a stable level. There was a significant difference in the temporal pattern of the ECFP/Venus emission ratio between the control and the $NaAsO_2$-exposed groups under serum-supplemented culture conditions [$F(12, 96) = 3.16$, $p < 0.001$].

In terms of the mean of the ECFP/Venus emission ratio in SCAT3-expressing PC12 cells during 80 to 180 min after exposure to $NaAsO_2$ there was no significant effect of culture condition [$F(1, 16) = 3.09$, $p = 0.10$], $NaAsO_2$ [$F(1, 16) = 0.81$, $p = 0.38$], or the interaction between these two main factors [$F(1, 16) = 0.002$, $p = 0.96$] (Fig. 2). However, two-way ANOVA indicated significant effects of $NaAsO_2$ [$F(1, 16) = 6.87$, $p < 0.05$] on the mean emission ratio during 200–300 min after exposure to $NaAsO_2$. Over this time period the effect of culture conditions [$F(1, 16) = 1.16$, $p = 0.30$] or the interactive effect of $NaAsO_2$ and culture conditions [$F(1, 16) = 0.17$, $p = 0.68$] was not significant. However, post hoc analysis indicated that the mean ECFP/Venus emission ratio was significantly ($p < 0.05$) increased by $NaAsO_2$ under serum-supplemented culture conditions, but not under serum-free culture conditions (Fig. 2).

3.2. Dose–response effects of $NaAsO_2$ on SCAT3-expressing cells

We next investigated the dose–response effects of $NaAsO_2$ on the ECFP/Venus emission ratio of SCAT3-expressing PC12 cells cultured in medium supplemented with serum. The fluorescence intensity of ECFP (*cyan blue*) and Venus (*yellow green*), as well as the morphology of SCAT3-expressing cells, were altered by exposure to $NaAsO_2$ at a concentration of 5 or 10 μM, whereas no dramatic changes in these parameters occurred in the control SCAT3-expressing PC12 cells or in the cells exposed to 1 μM $NaAsO_2$ (Fig. 3A; Supplementary data: Videos 1–4). The ratio of ECFP to Venus emission did not begin to change until 180 min after exposure to $NaAsO_2$ (Fig. 3B). The results by two-way ANOVA for repeated measures indicated that the temporal pattern of the ECFP/Venus emission ratio differed among the different groups [$F(36, 288) = 1.48$, $p < 0.05$]. In contrast analysis between groups, the temporal pattern of the ECFP/Venus emission ratio in the group exposed to 5 μM of $NaAsO_2$ significantly ($p < 0.005$) differed from that of the control group, but the ratio in the group exposed to 1 μM of $NaAsO_2$ did not. The ECFP/Venus emission ratio in the group exposed to 10 μM $NaAsO_2$ also changed over time in a similar manner to the change in the group exposed to 5 μM $NaAsO_2$. The difference in the temporal pattern of the ratio between the control group and the group exposed to 10 μM $NaAsO_2$ was close to significance ($p = 0.052$).

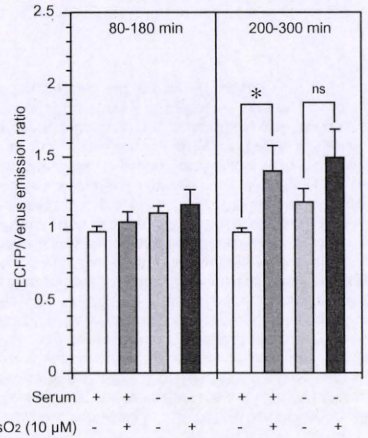

Fig. 2. Effects of $NaAsO_2$ and serum on the mean of the ECFP/Venus emission ratio of SCAT3-expressing PC12 cells. The ECFP/Venus emission ratio was calculated during 80–180 min or 200–300 min after exposure of SCAT3-expressing PC12 cells, in the presence or absence of serum, to the indicated concentrations of $NaAsO_2$. Values are the means ± SEM of five independent experiments. *, $p < 0.05$; ns, not significant.

Fig. 4 shows the means of the ECFP/Venus emission ratios during 80–180 min, and 200–300 min, after SCAT3-expressing PC12 cells were exposed to different doses of $NaAsO_2$. One-way ANOVA indicated that there was no significant difference in the mean of the ECFP/Venus emission ratio during 80–180 min after exposure of SCAT3-expressing PC12 cells to $NaAsO_2$ at any dose [$F(3, 24) = 0.98$, $p = 0.42$]. However, the mean of the ratio was significantly different among the groups [$F(3, 24) = 3.91$, $p < 0.05$] during 200–300 min after exposure. Post hoc analysis indicated that the mean of the ECFP/Venus emission ratio was significantly increased by 5 and 10 μM $NaAsO_2$ ($p < 0.01$ and $p < 0.05$, respectively), but not by 1 μM.

3.3. Effects of $NaAsO_2$ on the protein level of caspase-3

To compare the sensitivity and efficiency of the live imaging analysis of caspase-3 activation with SCAT3 to other assays of $NaAsO_2$-induced caspase-3 activation, we first assayed caspase-3 cleavage following exposure of PC12 cells to $NaAsO_2$ by Western blotting. The immunoreactive signals of cleaved caspase-3 protein (≈17 kDa), an active form of caspase-3, and uncleaved caspase-3 protein (≈32 kDa), were detected (Fig. 5). Exposure of PC12 cells to $NaAsO_2$ for 360 min did not significantly affect the amount of cleaved caspase-3 relative to the total amount of cleaved and uncleaved caspase-3 (Fig. 5A). In contrast, exposure to $NaAsO_2$ for 1200 min increased the level of cleaved caspase-3 and correspondingly decreased the level of uncleaved caspase-3 in a dose-dependent manner (Fig. 5B). The level of cleaved caspase-3 was significantly ($p < 0.0001$) increased by 1200-min exposure to 10 μM $NaAsO_2$.

3.4. Effects of $NaAsO_2$ on the activity of caspase-3

We next examined the enzymatic activity of caspase-3 by exposure of PC12 cells to $NaAsO_2$. Caspase-3 activity of PC12 cells was significantly increased by exposure to 10 μM $NaAsO_2$ for 360 and 1200 min ($p < 0.05$ and $p < 0.001$, respectively), while lower doses

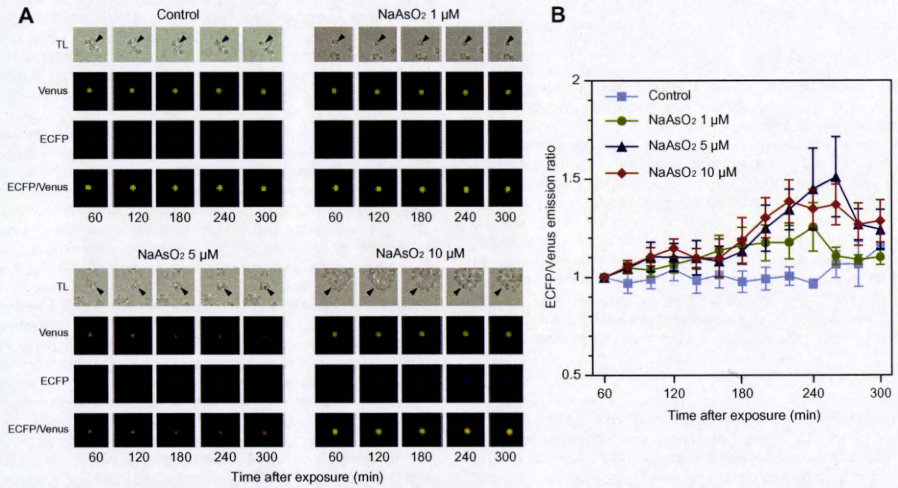

Fig. 3. Dose–response effects of $NaAsO_2$ on SCAT3-expressing PC12 cells under serum-supplemented culture conditions. A: Time-lapse images of SCAT3-expressing PC12 cells captured with transmitted light (TL), emissions of ECFP (*cyan blue*) and Venus (*yellow green*), and merged images of Venus and ECFP after conversion of fluorescent colors into pseudo colors (ECFP: *cyan blue* to *red*; Venus: *yellow green* to *green*). Arrowheads indicate SCAT3-expressing cells. B: Temporal changes in the ECFP/Venus emission ratio of SCAT3-expressing PC12 cells. The ratio at each time point was calibrated with the ratio at 60 min after arsenite exposure, which was set at 1. Values are the means ± SEM of five independent experiments. (For interpretation of the references to color in this figure legend, the reader is referred to the web version of this article.)

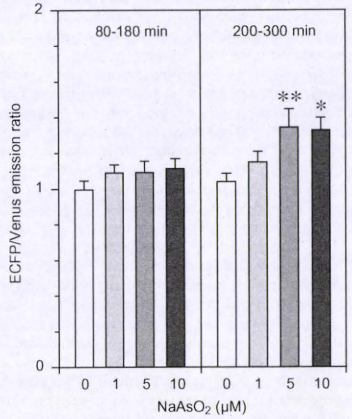

Fig. 4. Dose response effects of $NaAsO_2$ on the mean of the ECFP/Venus emission ratio of SCAT3-expressing PC12 cells under serum-supplemented culture conditions. The mean of the ECFP/Venus emission ratio was calculated during 80–180 min, or 200–300 min, after exposure to $NaAsO_2$ was initiated. Values are the means ± SEM of five independent experiments. **, $p < 0.01$ and *, $p < 0.05$ vs. control group (0 μM of $NaAsO_2$), respectively.

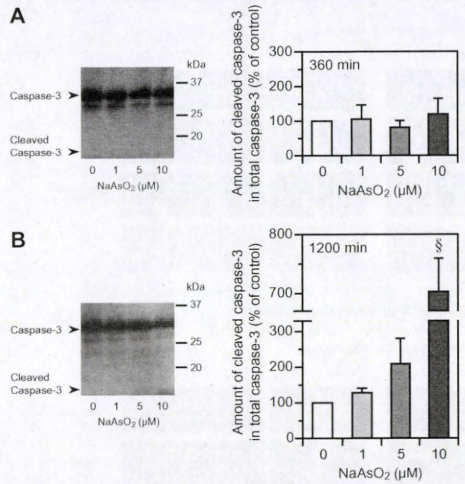

Fig. 5. Effect of $NaAsO_2$ on cleavage of the caspase-3 protein in PC12 cells following 360-min (A) or 1200-min (B) exposure to the indicated concentrations of $NaAsO_2$. The protein levels of capase-3 were assayed using Western blotting analysis. Immunoreactive caspase-3 bands are shown at left. Values are the means ± SEM of five independent experiments for the 360-min exposure and of four independent experiments for the 1200-min exposure.

of $NaAsO_2$ (1 and 5 μM) did not have any significant effects on caspase-3 activity (Fig. 6A and B). Exposure to 10 μM $NaAsO_2$ for 1200 min induced the highest increase in caspase-3 activity of PC12 cells, and this increased activity was completely blocked by the caspase inhibitor Z-VAD-FMK (Fig. 6B).

3.5. Effects of $NaAsO_2$ on DNA fragmentation

We next assessed the sensitivity of other assays of the cytotoxic effects of $NaAsO_2$ that determine $NaAsO_2$ effects on downstream effects of caspase activation. We first assayed the effect of $NaAsO_2$ on apoptosis by analysis of DNA fragmentation using an ELISA kit. The amount of nucleosomes generated from DNA fragmentation in PC12 cells was significantly ($p < 0.0001$) increased 1200 min after administration of 10 μM $NaAsO_2$ (Fig. 7). However, the amount of apoptotic nucleosomes in cells exposed to 1 or 5 μM $NaAsO_2$ was not significantly different from that of the control group.

3.6. Effects of $NaAsO_2$ on cell viability

We finally assayed the effect of $NaAsO_2$ on the viability of PC12 cells. No significant effect of $NaAsO_2$ on PC12 cell viability was observed one day after $NaAsO_2$ exposure was initiated (Fig. 8). However, cell viability was decreased on day 2 after $NaAsO_2$ exposure in a dose-dependent manner. Cell viability was significantly decreased by $NaAsO_2$ at doses of 5 or 10 μM ($p < 0.001$ or $p < 0.0001$, respectively), compared to that of the control group.

4. Discussion

Live imaging analysis of SCAT3-transfected cells using FRET technology is useful for monitoring the activity of caspase-3 (Takemoto et al., 2003; Kanuka et al., 2005; Kuranaga et al., 2006; Takemoto et al., 2007). The emission ratio of ECFP to Venus is elevated when the activation of caspase-3 is caused by death stimuli. We carried out live imaging of SCAT3-expressing PC12 cells and determined the temporal patterns of the emission ratio of ECFP to Venus as one step towards a proposed new method for cyto- and/or neuro-toxicity evaluation of environmental chemicals.

First, to determine the appropriate conditions for live imaging, we investigated the effects of culture conditions with or without serum-supplementation on the ECFP/Venus emission ratio during exposure to $NaAsO_2$. We observed an elevation in the ECFP/Venus emission ratio during 200–300 min after initiation of exposure to $NaAsO_2$ in the presence or absence of serum. However, under serum-free culture conditions, a significant difference in the ECFP/Venus emission ratio was not detected, because this ratio gradually increased in SCAT3-expressing PC12 cells even without exposure to $NaAsO_2$. The increase in this ratio without serum-supplementation or $NaAsO_2$ exposure may be due to the fact that serum deprivation induces cell death by apoptosis in PC12 cells (Greene, 1978; Morimoto et al., 2000; Shibano et al., 2002). The results of our current study indicate that the conditions of SCAT3-expressing cell culture are an important factor in evaluation of the cytotoxicity of chemicals. Thus, we found that culture of the cells in serum-supplemented medium is a prerequisite for the precise evaluation of the toxicity of chemicals by live imaging of SCAT3-expressing PC12 cells.

We next determined the dose–response relationship between $NaAsO_2$ and the ECFP/Venus emission ratio of SCAT3-expressing PC12 cells, which were cultured in medium supplemented with serum. The emission ratio of ECFP/Venus did not change until 180 min after exposure to $NaAsO_2$ at any dose, but afterwards this ratio increased with time. The mean of the ECFP/Venus emission ratio during 200–300 min after $NaAsO_2$ exposure was initiated was significantly increased by $NaAsO_2$ at a dose of 5 or 10 μM, but not at a dose of 1 μM. Accordingly, doses of 1 and 5 μM of

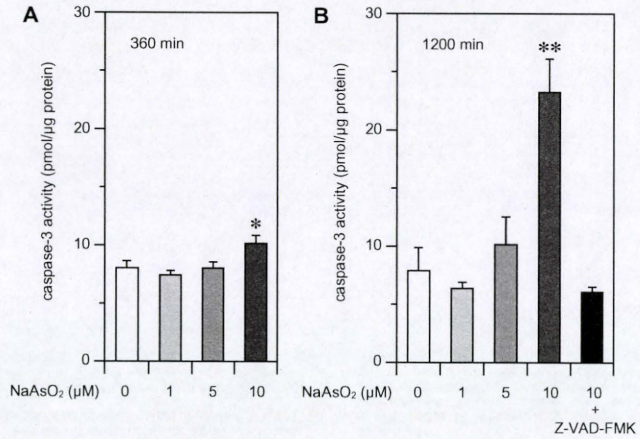

Fig. 6. Effects of $NaAsO_2$ on caspase-3 activity of PC12 cells. Cells were exposed to the indicated concentrations of $NaAsO_2$ for 360 min (A) or 1200 min (B). Caspase-3 activity of cell lysates was expressed as the amount of pNA (pmol) generated per protein (μg) extracted from the cells. Values are the means ± SEM of four or five independent experiments. **, $p < 0.001$ and *, $p < 0.05$ vs. control group (0 μM of $NaAsO_2$), respectively.

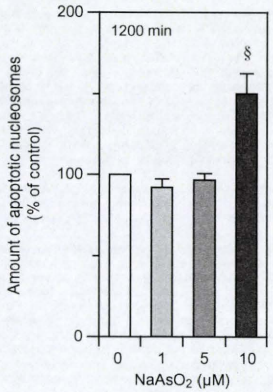

Fig. 7. Effects of $NaAsO_2$ on DNA fragmentation in PC12 cells. The level of apoptotic nucleosomes in PC12 cells following 1200-min exposure to the indicated concentrations of $NaAsO_2$ was assayed using an ELISA. The amount of nucleosomes generated from DNA fragmentation is expressed relative to that of control cells (0 μM of $NaAsO_2$) whose value was set at 100%. Values are the means ± SEM of four independent experiments. §, $p < 0.0001$ vs. control group (0 μM of $NaAsO_2$).

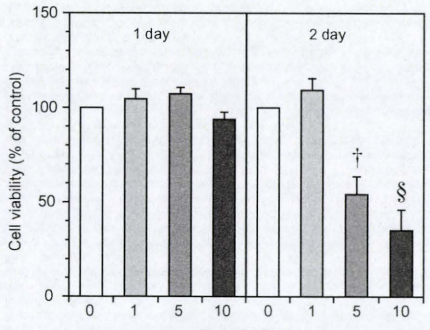

Fig. 8. Effects of $NaAsO_2$ on the viability of PC12 cells. PC12 cells were exposed to the indicated concentrations of $NaAsO_2$ for 1 or 2 days. The viability of PC12 cells was expressed relative to the viability of cells without $NaAsO_2$ exposure, whose value was set at 100%. Values are the means ± SEM of six independent experiments. † and §, $p < 0.001$ and $p < 0.0001$ vs. control group (0 μM of $NaAsO_2$).

$NaAsO_2$ may be defined as the no-observed-adverse-effect level (NOAEL) and lowest-observed-adverse-effect level (LOAEL), respectively, in which the adverse effect is defined as death of PC12 cells by apoptosis. Our findings suggest that live imaging analysis using SCAT3 is a suitable method for determination of the toxicity of chemicals.

SCAT3 is composed of a caspase-3 cleavage peptide sequence linking two fluorescent proteins (Takemoto et al., 2003). Increases in the emission ratio of ECFP to Venus in SCAT3-expressing PC12 cells therefore indicate that activation of caspase-3 occurs during $NaAsO_2$-induced death of PC12 cells. In fact, our current study showed that $NaAsO_2$ increases the protein level and enzymatic activity of the cleaved form of caspase-3 and facilitates DNA-fragmentation. Moreover, the increased activity of caspase-3 induced in PC12 cells by 10 μM of $NaAsO_2$ was completely suppressed by an inhibitor of caspases. Based on our combined results, we can conclude that $NaAsO_2$ induces apoptotic death of PC12 cells via activation of caspase-3.

Analysis of caspase-3 activation by western blotting of caspase-3 cleavage, by assay of caspase-3 activity, and also by live imaging of SCAT3-expressing cells, suggests that $NaAsO_2$ activates caspase-3, followed by induction of apoptotic cell death. However, western blotting analysis required a longer exposure time and a higher dose of $NaAsO_2$ to detect significant effects. A significant increase in the protein level of active caspase-3 was observed when PC12 cells were exposed to 10 μM of $NaAsO_2$ for 1200 min, but not when the cells were exposed to 10 μM of $NaAsO_2$ for 360 min, or when the cells were exposed to lower doses of $NaAsO_2$ for 1200 min. Similar results have been reported using human neuroblastoma SH-SY5Y cells, in which the level of active caspase-3 was significantly increased by exposure to $NaAsO_2$ (50 μM) for 1440 min, but not for 360 min (Watcharasit et al., 2008). In the present study, when we assayed caspase-3 activation using a caspase-3 activity assay, we observed a slight, but significant, increase in the caspase-3 activity of PC12 cells when the cells were exposed to 10 μM of $NaAsO_2$ for 360 min. However, such an increase did not occur following exposure to 5 μM of $NaAsO_2$. Another study that assayed caspase-3 activation using a caspase-3 activity assay showed that a significant increase in the activity of caspase-3 in PC12 cells is induced by exposure to 8 μM of arsenic trioxide for 1440 min (Piga et al., 2007). In contrast to the above methods of assay of caspase activation, live imaging analysis of SCAT3-expressing PC12 cells could rapidly detect significant effects of exposure to $NaAsO_2$ not only at 10 μM, but also at 5 μM. Thus, significant increases in the ECFP/Venus emission ratio occurred within 300 min after exposure to $NaAsO_2$ at doses of both 5 and 10 μM. Based on the combined data, we propose that live imaging analysis using SCAT3-expressing cells is a more sensitive and more efficient method for detection of cell death via caspase-3 activation than other methods. The only drawback that needs to be addressed is that it is difficult to precisely compare the temporal effects of $NaAsO_2$ on SCAT3-expressing PC12 cells of live imaging with the cumulative effects of exposure of PC12 cells to $NaAsO_2$ determined by other methods.

The use of the SCAT3-FRET technique enabled monitoring of the activity of caspase-3 at a single cell level as shown in Figs. 1 and 3, which would not be possible to do using Western blotting or caspase-3 activity assays. Furthermore, immunoreactive bands of active caspase-3 that were detected by Western blotting analysis were generally very weak. The only significant effect on caspase-3 activation that could be detected by Western blotting was when cells were exposed to 10 μM $NaAsO_2$ for 1200 min. These results indicate that the sensitivity of Western blotting analysis for detection of caspase-3 activation by $NaAsO_2$ is lower than that of live imaging analysis. Therefore, it may be necessary to obtain protein samples from a considerable number of cells for toxicity evaluation using Western blotting methods.

The SCAT3-FRET assay could be applied to a high throughput toxicity assay using a fluorescent microplate reader, although such an assay may decrease, or eliminate, the possibility of detection of the toxicity of chemicals at a single cell level. Live imaging analysis would not be more labor intensive than other methods since most fluorescent time-lapse microscopes, such as that used in the current study, can automatically image living cells. Thus, an improvement in the efficiency and accuracy of detection of chemical cytotoxic effects may be accomplished, at least in part, by live imaging analyses.

In the present study, we showed that exposure of cells to $NaAsO_2$ for 1200 min significantly increased the amount of nucleosomes generated by DNA fragmentation in PC12 cells at a dose of 10 μM $NaAsO_2$ but not at smaller doses. Moreover, the results of the cell viability assay suggest that the cytotoxic effects of $NaAsO_2$ on PC12 cell viability could only be detected 2 days after exposure to $NaAsO_2$. Another study which assayed the effect of $NaAsO_2$ exposure on cell viability using the MTT assay reported that exposure to $NaAsO_2$ for 1440 min inhibited the viability of PC12 cells in a dose-dependent manner, and that its IC_{50} value was approximately 22 μM when assayed over the range of 0.1–100 μM (van Vliet et al., 2007). Other studies that used staining with the DNA dye Hoechst 33258 (bis-benzimide) as a measure of apoptosis, showed that 15–20% of the PC12 cells that were exposed to 15 μM of $NaAsO_2$ for 1440 min were killed by apoptosis but less than 5% of the cells were killed after an exposure of 480 min (Cai et al., 2006; Cai and Xia, 2008). It is known that caspase family members disassemble the nuclear lamina, which provides mechanical support to the cell nucleus and plays an essential role in chromatin organization. Disruption of the membrane is followed by degradation of the nuclear envelope (Kihlmark et al., 2001). It was reported that an uncleavable mutation of lamin causes a significant delay in the onset of chromatin condensation and DNA fragmentation in cells killed by apoptosis (Rao et al., 1996). These data indicate that activation of caspase-3 occurs prior to chromatin condensation and DNA fragmentation. Therefore, an apoptotic assay based on DNA fragmentation and cell viability would require a long time to determine whether or not exposure to $NaAsO_2$ has an adverse effect on cells.

Most of the chemicals discharged into the environment remain to be evaluated regarding their toxicity towards human life. Furthermore, to work out a hazard assessment for a myriad of environmental chemicals is a demanding task. Although the analysis of animal toxicology is a useful approach for assessment of chemical hazards, it takes a long time to evaluate the toxicity of a chemical in this way. We believe that live imaging analyses of cultured cells, which will enable screening of the toxicity of chemicals within a short time and with high accuracy, will greatly facilitate hazard assessment of environmental chemicals.

Acknowledgments

This work was supported in part by the Environment Technology Development Fund from the Ministry of the Environment Japan (KS-02) to S. Tsukahara and by a Health and Labour Sciences Research Grant to M. Kakeyama. We thank Dr. M. Miura (University of Tokyo, Tokyo, Japan) for providing the pcDNA-SCAT3 vector.

Appendix A. Supplementary data

Supplementary data associated with this article can be found, in the online version, at doi:10.1016/j.tiv.2010.07.022.

References

Araragi, S., Kondoh, M., Kawase, M., Saito, S., Higashimoto, M., Sato, M., 2003. Mercuric chloride induces apoptosis via a mitochondrial-dependent pathway in human leukemia cells. Toxicology 184, 1–9.
Azad, N., Iyer, A.K., Manosroi, A., Wang, L., Rojanasakul, Y., 2008. Superoxide-mediated proteasomal degradation of Bcl-2 determines cell susceptibility to Cr(VI)-induced apoptosis. Carcinogenesis 29, 1538–1545.
Bustamante, J., Dock, L., Vahter, M., Fowler, B., Orrenius, S., 1997. The semiconductor elements arsenic and indium induce apoptosis in rat thymocytes. Toxicology 118, 129–136.
Cai, B., Xia, Z., 2008. p38 MAP kinase mediates arsenite-induced apoptosis through FOXO3a activation and induction of Bim transcription. Apoptosis 13, 803–810.
Cai, B., Chang, S.H., Becker, E.B., Bonni, A., Xia, Z., 2006. p38 MAP kinase mediates apoptosis through phosphorylation of BimEL at Ser-65. J. Biol. Chem. 281, 25215–25222.
Carlisle, D.L., Pritchard, D.E., Singh, J., Patierno, S.R., 2000. Chromium(VI) induces p53-dependent apoptosis in diploid human lung and mouse dermal fibroblasts. Mol. Carcinog. 28, 111–118.
Chattopadhyay, S., Bhaumik, S., Nag Chaudhury, A., Das Gupta, S., 2002. Arsenic induced changes in growth development and apoptosis in neonatal and adult brain cells in vivo and in tissue culture. Toxicol. Lett. 128, 73–84.
Choi, M.K., Kim, B.H., Chung, Y.Y., Han, M.S., 2002. Cadmium-induced apoptosis in h9c2, a7r5, and c6-glial cell. Bull. Environ. Contam. Toxicol. 69, 335–341.
Close, A.H., Guo, T.L., Shenker, B.J., 1999. Activated human T lymphocytes exhibit reduced susceptibility to methylmercury chloride-induced apoptosis. Toxicol. Sci. 49, 68–77.
Columbano, A., Ledda-Columbano, G.M., Coni, P.P., Faa, G., Liguori, C., Santa Cruz, G., Pani, P., 1985. Occurrence of cell death (apoptosis) during the involution of liver hyperplasia. Lab. Invest. 52, 670–675.
Dong, S., Shen, H.M., Ong, C.N., 2001. Cadmium-induced apoptosis and phenotypic changes in mouse thymocytes. Mol. Cell Biochem. 222, 11–20.

Dong, S., Liang, D., An, N., Jia, L., Shan, Y., Chen, C., Sun, K., Niu, F., Li, H., Fu, S., 2009. The role of MAPK and FAS death receptor pathways in testicular germ cell apoptosis induced by lead. Acta Biochim. Biophys. Sin. (Shanghai) 41, 800–807.
Gambelunghe, A., Piccinini, R., Abbritti, G., Ambrogi, M., Ugolini, B., Marchetti, C., Migliorati, G., Balducci, C., Muzi, G., 2006. Chromium VI-induced apoptosis in a human bronchial epithelial cell line (BEAS-2B) and a lymphoblastic leukemia cell line (MOLT-4). J. Occup. Environ. Med. 48, 319–325.
Gennari, A., Cortese, E., Boveri, M., Casado, J., Prieto, P., 2003. Sensitive endpoints for evaluating cadmium-induced acute toxicity in LLC-PK1 cells. Toxicology 183, 211–220.
Greene, L.A., 1978. Nerve growth factor prevents the death and stimulates the neuronal differentiation of clonal PC12 pheochromocytoma cells in serum-free medium. J. Cell Biol. 78, 747–755.
Habeebu, S.S., Liu, J., Klaassen, C.D., 1998. Cadmium-induced apoptosis in mouse liver. Toxicol. Appl. Pharmacol. 149, 203–209.
Hill, R., Leidal, A.M., Madureira, P.A., Gillis, L.D., Waisman, D.M., Chiu, A., Lee, P.W., 2008. Chromium-mediated apoptosis: involvement of DNA-dependent protein kinase (DNA-PK) and differential induction of p53 target genes. DNA Repair (Amst.) 7, 1484–1499.
Homma-Takeda, S., Kugenuma, Y., Iwamuro, T., Kumagai, Y., Shimojo, N., 2001. Impairment of spermatogenesis in rats by methylmercury: involvement of stage- and cell-specific germ cell apoptosism. Toxicology 169, 25–35.
Hossain, K., Akhand, A.A., Kato, M., Du, J., Takeda, K., Wu, J., Takeuchi, K., Liu, W., Suzuki, H., Nakashima, I., 2000. Arsenite induces apoptosis of murine T lymphocytes through membrane raft-linked signaling for activation of c-Jun amino-terminal kinase. J. Immunol. 165, 4290–4297.
Iwama, K., Nakajo, S., Aiuchi, T., Nakaya, K., 2001. Apoptosis induced by arsenic trioxide in leukemia U937 cells is dependent on activation of p38, inactivation of ERK and the Ca^{2+}dependent production of superoxide. Int. J. Cancer 92, 518–526.
Jiang, X.H., Wong, B.C., Yuen, S.T., Jiang, S.H., Cho, C.H., Lai, K.C., Lin, M.C., Kung, H.F., Lam, S.K., 2001. Arsenic trioxide induces apoptosis in human gastric cancer cells through up-regulation of p53 and activation of caspase-3. Int. J. Cancer 91, 173–179.
Kanuka, H., Kuranaga, E., Takemoto, K., Hiratou, T., Okano, H., Miura, M., 2005. Drosophila caspase transduces Shaggy/GSK-3beta kinase activity in neural precursor development. EMBO J. 24, 3793–3806.
Kihlmark, M., Imreh, G., Hallberg, E., 2001. Sequential degradation of proteins from the nuclear envelope during apoptosis. J. Cell Sci. 114, 3643–3653.
Kuranaga, E., Kanuka, H., Tonoki, A., Takemoto, K., Tomioka, T., Kobayashi, M., Hayashi, S., Miura, M., 2006. Drosophila IKK-related kinase regulates nonapoptotic function of caspases via degradation of IAPs. Cell 126, 583–596.
Luo, K.Q., Yu, V.C., Pu, Y., Chang, D.C., 2001. Application of the fluorescence resonance energy transfer method for studying the dynamics of caspase-3 activation during UV-induced apoptosis in living HeLa cells. Biochem. Biophys. Res. Commun. 283, 1054–1060.
Morimoto, Y., Nishihira, J., Kemmotsu, O., Shibano, T., Gando, S., Shikama, H., 2000. Pentobarbital inhibits apoptosis in neuronal cells. Crit. Care Med. 28, 1899–1904.
Nagai, T., Ibata, K., Park, E.S., Kubota, M., Mikoshiba, K., Miyawaki, A., 2002. A variant of yellow fluorescent protein with fast and efficient maturation for cell-biological applications. Nat. Biotechnol. 20, 87–90.
Namgung, U., Xia, Z., 2001. Arsenic induces apoptosis in rat cerebellar neurons via activation of JNK3 and p38 MAP kinases. Toxicol. Appl. Pharmacol. 174, 130–138.
Pachauri, V., Saxena, G., Mehta, A., Mishra, D., Flora, S.J., 2009. Combinational chelation therapy abrogates lead-induced neurodegeneration in rats. Toxicol. Appl. Pharmacol. 240, 255–264.
Piga, R., Saito, Y., Yoshida, Y., Niki, E., 2007. Cytotoxic effects of various stressors on PC12 cells: involvement of oxidative stress and effect of antioxidants. Neurotoxicology 28, 67–75.
Rana, S.V., 2008. Metals and apoptosis: recent developments. J. Trace Elem. Med. Biol. 22, 262–284.
Rao, L., Perez, D., White, E., 1996. Lamin proteolysis facilitates nuclear events during apoptosis. J. Cell Biol. 135, 1441–1455.
Rehm, M., Dussmann, H., Janicke, R.U., Tavare, J.M., Kogel, D., Prehn, J.H., 2002. Single-cell fluorescence resonance energy transfer analysis demonstrates that caspase activation during apoptosis is a rapid process. Role of caspase-3. J. Biol. Chem. 277, 24506–24514.
Rudolf, E., Cervinka, M., 2006. The role of intracellular zinc in chromium(VI)-induced oxidative stress, DNA damage and apoptosis. Chem. Biol. Interact. 162, 212–227.
Russo, P., Catassi, A., Cesario, A., Imperatori, A., Rotolo, N., Fini, M., Granone, P., Dominioni, L., 2005. Molecular mechanisms of hexavalent chromium-induced apoptosis in human bronchoalveolar cells. Am. J. Respir. Cell Mol. Biol. 33, 589–600.
Shabani, A., Rabbani, A., 2000. Lead nitrate induced apoptosis in alveolar macrophages from rat lung. Toxicology 149, 109–114.
Shenker, B.J., Guo, T.L., Shapiro, I.O.I.M., 1999. Induction of apoptosis in human T-cells by methyl mercury: temporal relationship between mitochondrial dysfunction and loss of reductive reserve. Toxicol. Appl. Pharmacol. 157, 23–35.
Shibano, T., Morimoto, Y., Kemmotsu, O., Shikama, H., Hisano, K., Hua, Y., 2002. Effects of mild and moderate hypothermia on apoptosis in neuronal PC12 cells. Br. J. Anaesth. 89, 301–305.
Takemoto, K., Nagai, T., Miyawaki, A., Miura, M., 2003. Spatio-temporal activation of caspase revealed by indicator that is insensitive to environmental effects. J. Cell Biol. 160, 235–243.
Takemoto, K., Kuranaga, E., Tonoki, A., Nagai, T., Miyawaki, A., Miura, M., 2007. Local initiation of caspase activation in Drosophila salivary gland programmed cell death in vivo. Proc. Natl. Acad. Sci. USA 104, 13367–13372.
Toimela, T., Tahti, H., 2004. Mitochondrial viability and apoptosis induced by aluminum, mercuric mercury and methylmercury in cell lines of neural origin. Arch. Toxicol. 78, 565–574.
Tse, W.P., Cheng, C.H., Che, C.T., Lin, Z.X., 2008. Arsenic trioxide, arsenic pentoxide, and arsenic iodide inhibit human keratinocyte proliferation through the induction of apoptosis. J. Pharmacol. Exp. Ther. 326, 388–394.
Tse, W.P., Cheng, C.H., Che, C.T., Zhao, M., Fan, R.Q., Lin, Z.X., 2009. Realgar-mediated growth inhibition on HaCaT human keratinocytes is associated with induction of apoptosis. Int. J. Mol. Med. 24, 189–196.
Tyas, L., Brophy, V.A., Pope, A., Rivett, A.J., Tavare, J.M., 2000. Rapid caspase-3 activation during apoptosis revealed using fluorescence-resonance energy transfer. EMBO Rep. 1, 266–270.
van Vliet, E., Eskes, C., Stingele, S., Gartlon, J., Price, A., Farina, M., Ponti, J., Hartung, T., Sabbioni, E., Coecke, S., 2007. Development of a mechanistically-based genetically engineered PC12 cell system to detect p53-mediated cytotoxicity. Toxicol. In Vitro 21, 698–705.
Wang, S., Leonard, S.S., Ye, J., Ding, M., Shi, X., 2000. The role of hydroxyl radical as a messenger in Cr(VI)-induced p53 activation. Am. J. Physiol. Cell Physiol. 279, C868–C875.
Watcharasit, P., Thiantanawat, A., Satayavivad, J., 2008. GSK3 promotes arsenite-induced apoptosis via facilitation of mitochondria disruption. J. Appl. Toxicol. 28, 466–474.
Wong, H.K., Fricker, M., Wyttenbach, A., Villunger, A., Michalak, E.M., Strasser, A., Tolkovsky, A.M., 2005. Mutually exclusive subsets of BH3-only proteins are activated by the p53 and c-Jun N-terminal kinase/c-Jun signaling pathways during cortical neuron apoptosis induced by arsenite. Mol. Cell Biol. 25, 8732–8747.

Original Paper

Neuro
-endocrinology

Neuroendocrinology
DOI: 10.1159/000327541

Received: August 24, 2010
Accepted after revision: March 15, 2011
Published online: April 22, 2011

Effects of Aromatase or Estrogen Receptor Gene Deletion on Masculinization of the Principal Nucleus of the Bed Nucleus of the Stria Terminalis of Mice

Shinji Tsukahara[a] Mumeko C. Tsuda[b] Ryohei Kurihara[a] Yukinori Kato[a] Yoshiko Kuroda[a] Mariko Nakata[b] Kai Xiao[b] Kazuyo Nagata[b] Katsumi Toda[c] Sonoko Ogawa[b]

[a]Division of Life Science, Graduate School of Science and Engineering, Saitama University, Saitama City, [b]Laboratory of Behavioral Neuroendocrinology, Graduate School of Comprehensive Human Sciences, University of Tsukuba, Tsukuba, and [c]Department of Biochemistry, School of Medicine, Kochi University, Nankoku, Japan

Key Words
Aromatase · Estrogen receptor · Bed nucleus of the stria terminalis · Masculinization · Sexual dimorphism · Sexually dimorphic nucleus · Sexual differentiation

Abstract
The principal nucleus of the bed nucleus of the stria terminalis (BNSTp) is a sexually dimorphic nucleus, and the male BNSTp is larger and has more neurons than the female BNSTp. To assess the roles of neuroestrogen synthesized from testicular androgen by brain aromatase in masculinization of the BNSTp, we performed morphometrical analyses of the adult BNSTp in aromatase knockout (ArKO), estrogen receptor-α knockout (αERKO), and estrogen receptor-β knockout (βERKO) mice and their respective wild-type littermates. In wild-type littermates, the BNSTp of males had a larger volume and greater numbers of neuronal and glial cells than did that of females. The volume and neuron number of the BNSTp in ArKO and αERKO males and glial cell number of the BNSTp in αERKO males were significantly smaller than those of wild-type male littermates, and they were not significantly different from those in female mice with either gene knockout. In contrast, there was no significant morphological difference in the BNSTp between βERKO and wild-type mice. Next, we examined the BNSTp of ArKO males subcutaneously injected with estradiol benzoate (EB) on postnatal days 1, 2, and 3 (1.5 μg/day). EB-treated ArKO males had a significantly greater number of BNSTp neurons than did oil-treated ArKO males. The number of BNSTp neurons in EB-treated ArKO males was comparable to that in wild-type males. These findings suggested that masculinization of the BNSTp in mice involves the actions of neuroestrogen that was synthesized by aromatase and that this estrogen mostly binds to ERα during the postnatal period.

Introduction

Sexual differentiation of the brain in mammalian species, including rodents and primates, is affected by testicular androgen during development, and it results in the formation of sexually dimorphic nuclei within the central nervous system [1, 2]. The bed nucleus of the stria terminalis (BNST) of the limbic system includes a sub-

KARGER

Fax +41 61 306 12 34
E-Mail karger@karger.ch
www.karger.com

0028–3835/11/0000–0000$38.00/0

Accessible online at:
www.karger.com/nen

Shinji Tsukahara
Graduate School of Science and Engineering, Saitama University
255 Shimo-Okubo, Sakura-ku
Saitama City, Saitama 338-8570 (Japan)
Tel. +81 48 858 3420, E-Mail stsuka@mail.saitama-u.ac.jp

nucleus that exhibits morphological sex differences. This subnucleus, which is known as the principal nucleus of the BNST (BNSTp) or the medial part of the posteromedial subdivision of the BNST, is larger and has more neurons in males than in females in adult rats and adult mice [3–5]. The BNSTp of rat is involved in the regulation of masculine sexual behavior, because lesions of the BNSTp induce deficits in male behavioral expression [6, 7]. Accordingly, morphological sex differences in the BNSTp are responsible for the sex-specific functions of this nucleus. The vasopressinergic system of the BNST also exhibits sexual dimorphism; males have more vasopressinergic neurons [8], and this sexual dimorphism is involved in sex difference in regulation of aggressive behavior [9]. In humans, a component of the BNST, which is called the darkly staining posteromedial component of the BNST or the central part of the BNST (hereafter the BNSTc), also exhibits morphological sex differences: it is larger in men than in women [10, 11]. Furthermore, the volume and neuron number of the BNSTc in male-to-female transsexuals, but not in homosexual men, are comparable to those in heterosexual women [11, 12], suggesting that the BNSTc in humans is related to gender identity.

Neonatal castration in male rodents results in a decrease in the volume and neuron number of the BNSTp, while testosterone propionate injection in newborn females results in an increase in both [13, 14], indicating that the morphological sex differences in the BNSTp can be eliminated and reversed by manipulation with androgen during the neonatal period. In addition, BNSTp volume on the left side, but not on the right side, in testicular feminization mutation male rats, in which androgen receptors are less functional, is as small as that in normal female rats [15], suggesting that androgen binding to androgen receptors is implicated in masculinization of the BNSTp. Moreover, in rodents, it is generally accepted that perinatal testicular androgen exerts significant effects on organization of male-typical structures on the brain after it is converted to estrogen in the brain by the cytochrome P450 enzyme aromatase [1, 2], although sexual differentiation of the brain is proposed to be partially sex chromosome-dependent [16, 17]. Hisasue et al. [18] recently reported that treatment with estradiol benzoate (EB) or a selective agonist of estrogen receptor (ER)-α or -β into newborn female mice increases the number of neuron in the BNSTp and enlarges BNSTp volume in adulthood, although activation of either ERα or ERβ is not sufficient for masculinization of the BNSTp. Thus, estrogen actions via both ERα and ERβ may be required for masculinization of the BNSTp in mice. However, Hisasue et al. [18] also showed that neonatal EB treatment was ineffective in increasing BNSTp volume in female mice. Therefore, it remains unclear whether the estrogen that is synthesized from testicular androgen by aromatase has all the functions necessary for masculinization of the BNSTp in male mice.

To assess the role of aromatase in masculinization of the BNSTp, we examined the morphology of the BNSTp in both sexes of aromatase knockout (ArKO) mice. Similarly, we examined the morphology of the BNSTp in ERα knockout (αERKO) and ERβ knockout (βERKO) mice to assess the involvement of these ERs in BNSTp masculinization. We next examined the BNSTp of ArKO male mice treated with EB in the early postnatal period to determine whether this treatment could rescue the effects of an aromatase gene deletion on the BNSTp in males.

Animals and Methods

Animals

ArKO [19, 20], αERKO [21], and βERKO mice [22] and their respective wild-type littermates were obtained from litters resulting from matings between heterozygous mice derived from the respective breeding colonies, which were maintained at the University of Tsukuba. Mice from the breeding colonies were all completely backcrossed to C57BL/6J mice. All animals were housed in a room maintained at 22°C with a 12-hour light/12-hour dark lighting cycle (light on at 08:00 h) with free access to a standard diet and tap water. This study was performed in accordance with the National Institutes of Health guidelines and approved by the University of Tsukuba Animal Care and Use Committee.

Experimental Design

Experiment 1

Coronal brain sections obtained from male and female adult ArKO, αERKO, or βERKO mice and their respective wild-type littermates were stained with cresyl fast violet (ArKO male: n = 4 (17–20 weeks old); wild-type male littermate of ArKO mice: n = 4 (15–30 weeks old); ArKO female: n = 4 (17–21 weeks old); wild-type female littermate of ArKO mice: n = 4 (15–30 weeks old); αERKO male: n = 5 (15–27 weeks old); wild-type male littermate of αERKO mice: n = 6 (14–27 weeks old); αERKO female: n = 5 (13–32 weeks old); wild-type female littermate of αERKO mice: n = 4 (13–32 weeks old); βERKO male: n = 5 (13–25 weeks old); wild-type male littermate of βERKO mice: n = 4 (13–25 weeks old); βERKO female: n = 5 (13–20 weeks old); wild-type female littermate of βERKO mice: n = 5 (14–20 weeks old)). Using a stereological method (see below section 'Stereological Analysis of the BNSTp' for details), BNSTp volume and neuronal and glial cell numbers in the BNSTp were measured to determine the effects of aromatase, ERα, or ERβ gene deletions on masculinization of the BNSTp. Neuronal cell density in the BNSTp was calculated by dividing BNSTp volume with neuronal cell number; glial cell density was also calculated using this method. These cell densities were also assessed to determine the effects of aromatase, ERα, or ERβ gene deletions. Additionally, we measured testosterone concentrations in plasma, which were taken from animals used for histological analyses, by enzyme-linked immunosorbent assay to examine whether there was a causal relationship between the morphology of the BNSTp and testosterone levels in adulthood.

Experiment 2

We next examined whether the effects of the aromatase gene deletion on masculinization of the BNSTp can be rescued in ArKO male mice by postnatal treatment with estrogen. ArKO male mice (n = 6) and wild-type male mice (n = 3) were subcutaneously injected with 1.5 μg of EB dissolved in 5 μl of sesame oil on postnatal days 1, 2, and 3 (postnatal day 1 = day of birth). As a negative control, sesame oil (5 μl/day) was injected into ArKO male mice (n = 4) and wild-type male mice (n = 5) on the same days as the EB injection. Postnatal treatment with 7.5- or 15-μg of 17β-estradiol restores reproductive ability and aggressive behavior in ArKO male mice [20, 23], and the binding affinity of EB to murine ERα is approximately 6–10 times higher than that of 17β-estradiol [24]. We referred to these reports to determine the dose of EB used in this experiment.

After sexual maturation of these animals (17–21 weeks), coronal brain sections that included the BNSTp were stained with cresyl fast violet, and the volume of the BNSTp and the neuronal and glial cell numbers in the BNSTp were measured using a stereological method (see below section 'Stereological Analysis of the BNSTp' for details). The densities of neuronal and glial cells in the BNSTp were measured described above. The densities were also assessed to determine the effects of postnatal EB treatment on the BNSTp of ArKO males.

General Procedures

Specimen Preparation

Animals deeply anesthetized with sodium pentobarbital (60 mg/kg body weight) were perfused intracardially with 0.1 M phosphate-buffered saline (PBS; pH 7.5), followed by 4% paraformaldehyde in 0.1 M phosphate buffer (PB; pH 7.5). Brains were post-fixed at 4°C overnight with 4% paraformaldehyde in 0.1 M PB and then immersed in 30% sucrose in 0.1 M PB for 2 days at 4°C. Coronal brain sections (30 μm thickness) that included the BNSTp were prepared with a cryostat and collected from rostral to caudal levels of the BNSTp at 60-μm intervals.

Brain sections were mounted on gelatin-coated slides, placed in a graded series of ethanol solutions for delipidation, and then stained with 0.1% cresyl fast violet solution for 5–10 min. The sections were placed in distilled water, sequentially incubated in a graded series of ethanol solutions appropriate for bleaching of the dye, dehydrated with absolute ethanol, cleared with xylene, and covered with embedding medium and a coverslip. The stained sections were used for stereological analysis.

Stereological Analysis of the BNSTp

We observed the BNSTp of cresyl-fast-violet-stained sections (thickness 30 μm/section, collecting interval 60 μm) on a PC monitor with the aid of a CCD camera connected to a light microscope (DM5000B; Leica Microsystems, Wetzlar, Germany) and measured BNSTp volume and the numbers of neuronal and glial cells in the BNSTp with the aid of a computer and Stereo Investigator software (MBF Bioscience, Inc., Williston, Vt., USA). To avoid bias, identification numbers of animals were coded, and the person who performed the stereological analysis was blinded to the source of the materials. In this study, we analyzed the BNSTp on the left side because the BNSTp on the left side is known to be larger than that on the right and because the sex difference in BNSTp volume is prominent on the left side [15]. The rostro-caudal levels of brain sections used in analysis were from the septo-preoptic region to the anterior hypothalamic region, and the region of interest corresponded to the posteromedial part of the medial division of the BNST (BSTMPM) described in the mouse brain atlas by Paxinos and Franklin [25]. The average numbers of sections collected per animal were as follows: 5.5 for males and 6 for females among ArKO mice and their wild-type littermates, 6.7 for males and 6 for females among αERKO and their wild-type mice, and 4.9 for males and 4 for females among βERKO and their wild-type mice in experiment 1, and 4.9 per animal in experiment 2.

To measure BNSTp volume and neuronal and glial cell numbers in the BNSTp on the left side, we used the optical fractionator method in accordance with the system workflow of the Stereo Investigator (MBF Bioscience, Inc.). Briefly, we traced outlines of the BNSTp on the images of the sections to calculate the estimated volume of the BNSTp and select the region for cell counts. After setting the counting frame size to 20 × 20 μm, the grid size for arrangement of the counting frame at 200 × 200 μm, the highest optical dissector setting at 10–12 μm, and the highest top guard zone setting at 2–4 μm, neuronal and glial cells within the counting frames were then counted manually to estimate the total numbers of neuronal and glial cells in the BNSTp. As the criteria for counting neurons, cells containing blue- or purple-colored rough endoplasmic reticulum (Nissl bodies) in the cytoplasm and having an oval or spherical nucleus with a blue- or purple-colored nucleolus were defined as neuronal cells. For measuring the number of glial cells, we counted cells that had blue- or purple-colored nucleus without colored cytoplasm, excepting cells contacting capillary wall.

Enzyme-Linked Immunosorbent Assay for Testosterone

Blood was taken from the right atrium before animals were perfused with PBS for histological processing (see *Specimen Preparation*). The lipophilic fraction of the plasma was extracted with diethyl ether according to a procedure described previously [26]. Testosterone in extracted samples was assayed using a Testosterone EIA Kit (Cayman Chemical, Ann Arbor, Mich., USA) in accordance with the manufacturer's protocol. The intra- and inter-assay coefficients of variation were 5.9% (testosterone concentration, 143.4 pg/ml) and 10.7% (testosterone concentration, 68.5 pg/ml), respectively.

Statistical Analyses

Two-way analysis of variance (ANOVA) was used to determine the main effects of genotype and sex, and the effects of interaction between genotype and sex on BNSTp volume, neuronal and glial cell numbers, neuronal and glial cell densities, and plasma testosterone concentration in experiment 1. Two-way ANOVA was also preformed to determine main effects of hormonal treatment and sex and effects of interaction between hormonal treatment and sex on BNSTp volume, neuronal and glial cell numbers, and neuronal and glial cell densities. When significant effects of an interaction between main factors were detected by two-way ANOVA, Fisher's PLSD test was performed for post-hoc analysis. In the post-hoc analysis, a probability value of $p < 0.05$ was considered significant.

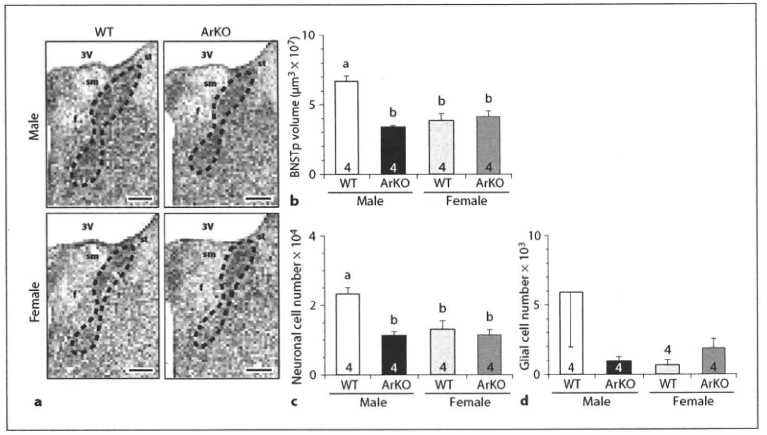

Fig. 1. Effects of the aromatase gene deletion on the BNSTp of mice. Photomicrographs of the BNSTp in cresyl-fast-violet-stained coronal brain sections of ArKO and wild-type (WT) mice (**a**). Dashed line in each panel indicates the outline of the BNSTp. Scale bars indicate 300 μm. f, fornix; sm, stria medullaris of thalamus; st, stria terminalis; 3V, third ventricle. BNSTp volume (**b**) numbers of neuronal cells (**c**) and glial cells (**d**) in the BNSTp of ArKO mice and their wild-type littermates. The number in each column indicates the number of animals used. Values (mean ± SEM) with different letters differ significantly ($p < 0.05$) from each other.

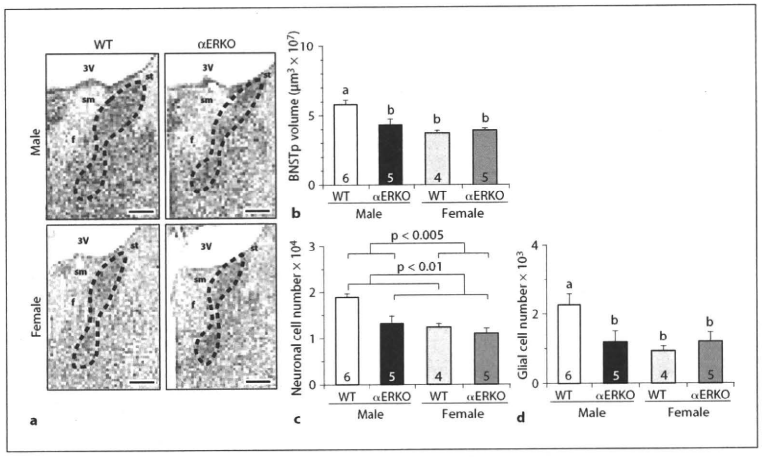

Fig. 2. Effects of the ERα gene deletion on the BNSTp of mice. Photomicrographs of the BNSTp in cresyl-fast-violet-stained coronal brain sections of αERKO and WT mice (**a**). BNSTp volume (**b**) numbers of neuronal cells (**c**) and glial cells (**d**) in the BNSTp of αERKO mice and their wild-type littermates. The number in each column indicates the number of animals used. Values (mean ± SEM) with different letters differ significantly ($p < 0.05$) from each other. Scale bars indicate 300 μm. See figure 1 for abbreviations.

Results

Experiment 1

Effects of Deletion of the Aromatase Gene on BNSTp

The BNSTp, which was occupied with cresyl-fast-violet-stained neuronal cell bodies in specimen preparations, was larger in wild-type males than in wild-type females (fig. 1a). In contrast, the size of the BNSTp in ArKO male mice was comparable to that in ArKO female mice and was smaller than that in male wild-type littermates. Stereological analysis revealed that the aromatase gene deletion decreased the BNSTp volume in male but not in female mice (fig. 1b). Two-way ANOVA indicated that there were significant effects of genotype ($F_{1, 12} = 17.8$, $p < 0.005$) and of sex ($F_{1, 12} = 7.92$, $p < 0.05$) on BNSTp volume among ArKO mice and their wild-type littermates. The effect of an interaction between genotype and sex was significant ($F_{1, 12} = 24.0$, $p < 0.0005$). Based on post-hoc analysis, BNSTp volume in wild-type males was significantly larger than that in wild-type females. In contrast, there was no significant difference in BNSTp volume between the sexes in ArKO mice, and this apparent similarity was due to a significant reduction in BNSTp volume of ArKO males.

The aromatase gene deletion decreased not only BNSTp volume but also neuronal cell number in the BNSTp of males (fig. 1c). There were significant effects of genotype ($F_{1, 12} = 15.1$, $p < 0.005$), of sex ($F_{1, 12} = 7.87$, $p < 0.05$), and of an interaction between genotype and sex ($F_{1, 12} = 8.34$, $p < 0.05$) on the neuron number among ArKO mice and their wild-type littermates. Based on the post-hoc analysis, the number of neurons in the BNSTp of ArKO males was significantly smaller than that in wild-type male littermates, while there was no significant difference in the neuron number between ArKO females and their wild-type female littermates. There was no significant difference in the neuron number between male and female ArKO mice, and this apparent similarity was due to a significant reduction of the number of neurons of ArKO males.

The number of glial cells in the BNSTp did not significantly differ by sex or genotype among ArKO mice and their wild-type littermates (fig. 1d). There was no effect of an interaction between sex and genotype on the number of glial cells in the BNSTp, although the glial cell number had tendency to be larger in the wild-type male littermates. There was no significant effect of genotype, of sex, or of an interaction between genotype and sex on neuronal and glial cell densities in the BNSTp among ArKO mice and their wild-type littermates (data not shown).

Effects of Deletion of the ERα Gene on BNSTp

Based on images from the light microscope, the BNSTp was thinner along the mediolateral axis in αERKO males than in wild-type males, although no apparent difference in the morphology of BNSTp was found between αERKO females and wild-type females (fig. 2a). Based on measurement of BNSTp volume, we found significant effects of genotype ($F_{1, 16} = 5.49$, $p < 0.05$), of sex ($F_{1, 16} = 20.2$, $p < 0.0005$), and of an interaction between genotype and sex ($F_{1, 16} = 9.55$, $p < 0.01$) among αERKO mice and their wild-type littermates. Based on post-hoc analysis, BNSTp volume was significantly larger in wild-type males than in wild-type females (fig. 2b). Moreover, BNSTp volume in αERKO male mice was significantly smaller than that in wild-type males and did not significantly differ from that in female mice.

Among αERKO mice and their wild-type littermates, neuron number in the BNSTp in αERKO males was lower than that of the wild-type males and similar to that of females (fig. 2c). Two-way ANOVA indicated that there were significant effects of genotype ($F_{1, 16} = 10.3$, $p < 0.01$) and of sex ($F_{1, 16} = 15.1$, $p < 0.005$) on the number of neurons in the BNSTp, though the effect of the interaction between genotype and sex was not significant. There was no significant effect of genotype, of sex, or of the interaction between genotype and sex on the density of neurons in the BNSTp among αERKO mice and their wild-type littermates (data not shown).

The ERα gene deletion decreased not only BNSTp volume and neuron number but also glial cell number in the BNSTp of mutant males (fig. 2d). There were significant effects of sex ($F_{1, 16} = 5.23$, $p < 0.05$) and of an interaction between genotype and sex ($F_{1, 16} = 5.47$, $p < 0.05$) on the glial cell number among αERKO mice and their wild-type littermates, although the overall effect of genotype was not significant. Based on the post-hoc analysis,

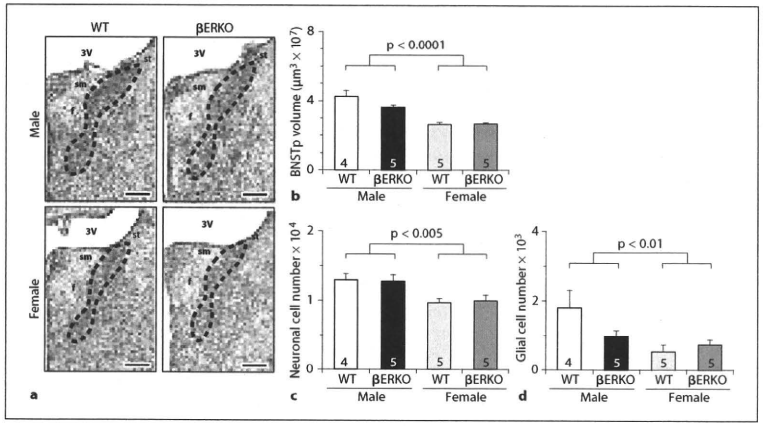

Fig. 3. Effects of the ERβ gene deletion on the BNSTp of mice. Photomicrographs of the BNSTp in cresyl-fast-violet-stained coronal brain sections of βERKO and WT mice (**a**). BNSTp volume (**b**) numbers of neuronal cells (**c**) and glial cells (**d**) in the BNSTp of βERKO mice and wild-type littermates. The number in each column indicates the number of animals used. Values are the mean ± SEM. Scale bars indicate 300 μm. See figure 1 for abbreviations.

αERKO males had a significantly smaller number of glial cells in the BNSTp than did the wild-type males, and the number in αERKO males was similar to and not significantly different from that in wild-type and αERKO females. However, the density of glial cells in the BNSTp was not affected by sex, genotype, or an interaction between sex and genotype (data not shown).

Effects of Deletion of the ERβ Gene on BNSTp

The BNSTp was larger and had greater neuronal and glial cell numbers in the βERKO males and their wild-type male littermates than in the βERKO females and their wild-type female littermates (fig. 3). We observed a significant effect of sex on BNSTp volume ($F_{1, 15} = 55.4$, $p < 0.0001$), neuronal cell number in the BNSTp ($F_{1, 15} = 12.8$, $p < 0.005$), and glial cell number in the BNSTp ($F_{1, 15} = 8.78$, $p < 0.01$) among βERKO and wild-type mice. However, the values of these endpoints were not significantly changed by genotype or by an interaction between sex and genotype. There was no significant effect of genotype, of sex, or of an interaction between genotype and sex on neuronal and glial cell densities in the BNSTp among βERKO mice and their wild-type littermates (data not shown).

Plasma Testosterone Levels in ArKO, αERKO, and βERKO Mice

Plasma testosterone concentrations were higher in males than in females, and the levels of plasma testosterone were higher in ArKO animals (fig. 4a). Two-way ANOVA revealed that there were significant effects of sex ($F_{1, 12} = 13.8$, $p < 0.005$) and genotype ($F_{1, 12} = 38.2$, $p < 0.0001$) on plasma testosterone concentrations among ArKO mice and their wild-type littermates. However, plasma testosterone level was not affected by an interaction between genotype and sex.

We found a significant effect of genotype on plasma testosterone concentrations among αERKO mice and wild-type littermates ($F_{1, 16} = 26.7$, $p < 0.0001$). Deletion of the ERα gene increased testosterone levels in both sexes, and the testosterone levels in αERKO females was comparable to those in αERKO males (fig. 4b).

βERKO males and their wild-type male littermates had significantly higher concentrations of plasma testosterone than did their βERKO and wild-type female littermates ($F_{1, 15} = 16.6$, $p < 0.005$) (fig. 4c). On the other hand, deletion of the ERβ gene did not significantly change plasma testosterone levels in either sex. Two-way ANOVA indicated that neither genotype nor an interaction between sex and genotype significantly affected plasma testosterone levels.

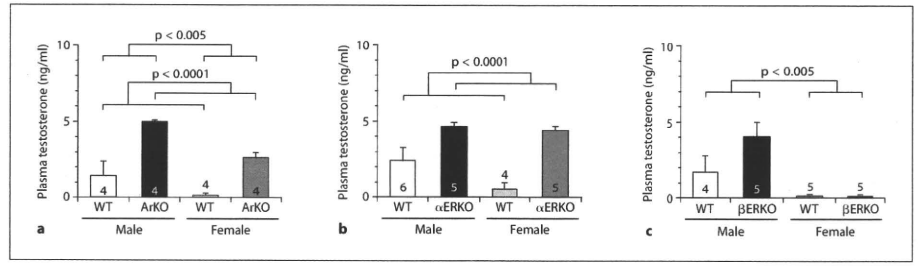

Fig. 4. Effects of the aromatase, ERα, or ERβ gene deletions on plasma testosterone concentration in mice. Plasma testosterone concentrations of ArKO mice (**a**), αERKO mice (**b**), and βERKO mice (**c**). Values are the mean ± SEM. The number in each column indicates the number of animals used.

Experiment 2

We examined the effects of postnatal EB treatment on the BNSTp in ArKO and wild-type adult male mice and found that there was no significant effect of postnatal EB treatment or of an interaction between hormonal treatment and genotype. However, two-way ANOVA revealed significant differences in BNSTp volume between ArKO and wild-type males ($F_{1, 14} = 27.9$, $p < 0.0005$). BNSTp volume was smaller in ArKO males than in wild-type males (fig. 5a).

Neuronal cell number in the BNSTp was significantly changed by an interaction between genotype and hormonal treatment ($F_{1, 14} = 5.56$, $p < 0.05$), although no significant effect of either main factor alone was found. Based on post-hoc analysis, oil-treated wild-type males had a significantly greater number of neurons in the BNSTp than did oil-treated ArKO males (fig. 5b). Postnatal EB treatment significantly increased neuron number in the BNSTp of ArKO males, but not in the wild-type males. There was a significant effect of genotype on neuronal cell density in the BNSTp among ArKO and wild-type males with or without postnatal EB treatment ($F_{1, 14} = 6.22$, $p < 0.05$), and the density of ArKO males was higher than that of the wild-type males (fig. 5c).

The number of glial cells in the BNSTp did not significantly differ among ArKO and wild-type male mice with or without EB treatment (fig. 5d). The density of glial cells in the BNSTp was not significantly different among ArKO and wild-type males with or without EB treatment (fig. 5e).

Discussion

The BNSTp is a sexually dimorphic nucleus that is larger and contains more neurons in male rodents than in female rodents [3–5]. We confirmed this sexual dimorphism in wild-type littermates of ArKO, αERKO, and βERKO mice. Our study further showed that the sexual dimorphism in the volume and neuron number of the BNSTp was completely eliminated in ArKO mice. This elimination of sexual dimorphism was entirely due to a significant reduction in the volume and neuron number of the BNSTp in ArKO males, and not to changes in ArKO females. These findings indicated that aromatase played an essential role in the formation of the male-typical structure of the BNSTp. The BNST contains more arginine-vasopressin neurons in males than in females [8]. The number of arginine-vasopressin neurons in the BNST of ArKO male mice is smaller than that of the wild-type males [27]. Reduction of neuron number in the BNSTp of ArKO males may be caused, in part, by a decrease in arginine-vasopressin neurons. Aromatase is an enzyme that converts androgen to estrogen. Therefore, it is likely that the aromatase deficiency results in a loss of estrogen function. As we expected, elimination of the sex difference in the volume and neuron number of the BNSTp occurred not only in ArKO mice but also in αERKO mice, which was due to a reduction of the volume and neuron number in knockout male mice rather than to changes in female mice. αERKO mice used in this study are known to have a small number of ERα-containing cells in the medial preoptic area, but not in other regions of the brain, including the BNST [28], indicating

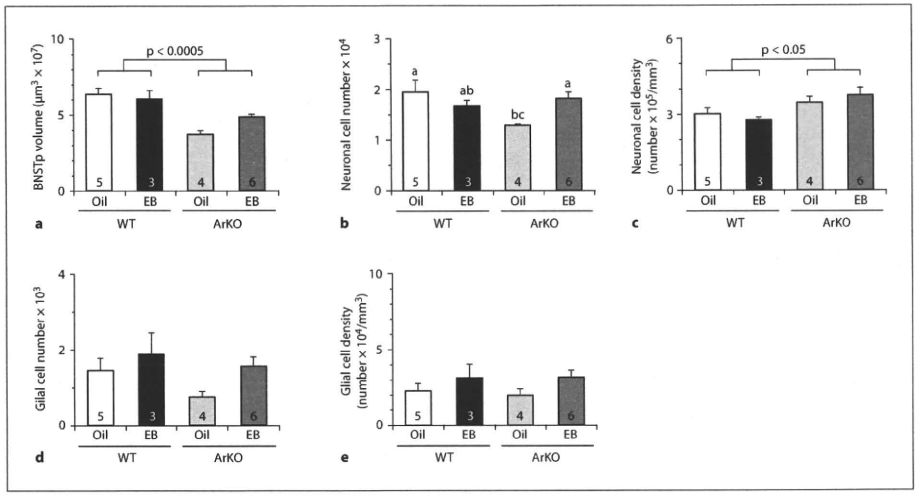

Fig. 5. Effects of postnatal EB treatment on BNSTp volume (**a**), the number and density of neuronal cells (**b**, **c**) and the number and density of glial cells (**d**, **e**) in the BNSTp of ArKO male mice. The number of animals used in each group is indicated in each column. Values (mean ± SEM) with different letters differ significantly ($p < 0.05$) from each other.

that the αERKO mice do not completely lack ERα expression in the brain. Morphological alteration in the BNSTp of αERKO males may be mainly due to the lack of ERα within the BNSTp. In contrast, the volume and neuron number of the BNSTp did not change with deletion of the ERβ gene, and βERKO mice exhibited morphological sex differences in the BNSTp as did the wild-type littermates. Taken together, the findings of our current study suggested that the actions of estrogen synthesized from androgen by aromatase were essential for organization of male-typical structures in the BNSTp of mice and that the actions of this estrogen are mostly mediated through its binding to ERα rather than to ERβ.

In the current study, we also found a sex difference in glial cell number in the BNSTp of mice. Morphometrical analysis demonstrated that the number of glial cells was significantly greater in the male BNSTp than in the female BNSTp in the wild-type littermates of αERKO and βERKO mice. Furthermore, this sex difference was eliminated by deletion of the ERα gene, but not the ERβ gene. Based on these findings, we believe that sex difference in glial cell number contributed to the sexual dimorphism of the BNSTp, at least in part, and that estrogen actions via ERα were involved in producing sex difference in glial cell number. However, among ArKO mice and the wild-type littermates, we did not observe a significant effect of sex or genotype on glial cell number in the BNSTp, although the number of glial cells tended to be higher in wild-type males than in wild-type females and ArKO males. In addition, no significant difference in the number of GFAP-immunoreactive cells was reported in the BNSTp of mice [29]. Further study is needed to determine whether and how sex differences in glial cell number arise in the BNSTp.

In rodent models of sexual dimorphism, masculinization and defeminization of the brain involve the actions of estrogen, which is synthesized locally in the brain from testicular androgen by aromatase during the perinatal period [1, 2]. In this context and as shown in this study, it is likely that the morphological sex differences in the BNSTp of mice are eliminated by a deletion of the aromatase gene. In this study, we also examined whether postnatal EB treatment rescued the effects of the aromatase gene deletion on the BNSTp of ArKO male mice. We found that postnatal EB treatment significantly increased the number of neurons in the BNSTp of ArKO males and that the neuron number in EB-treated ArKO males was similar to that of the wild-type males. This finding suggested that estrogen functions during the early postnatal period to maintain neuron number of the BNSTp in male mice. Also, in female mice, postnatal EB treatment has been shown to increase the number of BNSTp neurons [18]. Neurons expressing aromatase are located in the BNSTp of rats during the late prenatal period to the early postnatal period [30]. Cellular colocalization of ERα and aromatase has been reported in the BNST of mice in the postnatal period [31]. These results suggest that maintenance of the number of BNSTp neurons in male mice may involve the effects of estrogen, which is locally produced by aromatase and binds to ERα in BNSTp in the postnatal period.

EB treatment in the early postnatal period significantly increased the number of BNSTp neurons in ArKO males to a level comparable to that in wild-type males. However, EB-treated ArKO males had a significantly smaller BNSTp volume than did wild-type males. This last observation indicated that the hormonal treatment used in this study was not sufficient to reverse the effects of an aromatase gene deletion. It is unclear why the EB treatment did not result in a complete recovery of BNSTp volume. Also, a study using female mice did not clearly determine whether postnatal EB treatment can masculinize the volume of female BNSTp because it showed that BNSTp volume in adulthood was increased by subcutaneous injection of EB into newborn females, but it also showed no effect of this same treatment [18]. However, this previous report clearly demonstrated that EB treatment could increase the number of BNSTp neurons in female mice [18]. There are several possible hypotheses that could explain why postnatal EB treatment did not restore BNSTp volume in male ArKO mice. First, differences in the effects of EB between BNSTp volume and neuron number would be explained if neuronal cell size were smaller in EB-treated ArKO males even though neuron number had increased. Sex difference in BNSTp volume is due to sex differences in cell number and cell size because cells are larger in the BNSTp of male mice than that of female mice [3]. Alternatively or additionally, the timing of EB treatment may be appropriate for recovery of neuron number but not for recovery of BNSTp volume. In ferrets, pharmacological blockade of estrogenic actions during the prenatal period suppresses masculine sexual behavior [32] and disrupts the male-typical formation of a sexually dimorphic nucleus of the preoptic/anterior hypothalamic area [33]. Such evidence suggests that prenatal, rather than postnatal, EB treatment may be able to recover BNSTp volume in ArKO males; however, our study did not test this possibility. It is also possible that estrogen exerting its actions during the perinatal period was not sufficient for complete masculinization of the BNSTp, for example, a sensitive period important for organizational actions of sex steroids may begin during the perinatal period and end in late adolescence [34].

Reportedly, ArKO mice have higher circulating levels of testosterone than do wild-type mice of both sexes [20, 35]. αERKO mice also have higher blood testosterone concentrations than wild-type mice [36–39]. We confirmed that the circulating levels of testosterone are elevated in both ArKO and αERKO mice. When considering the effects of deletion of the aromatase or ERα gene on the BNSTp and on circulating testosterone levels, it is reasonable to think that the morphometrics of the BNSTp, such as volume and neuronal and glial cell numbers, are not altered by circulating testosterone levels in adulthood. However, it was reported that androgen affects the medial amygdala of adult rats to increase the volume, neuronal soma size, and number of glial cells [40].

Apoptosis during the postnatal period may contribute to sex differences in neuron numbers in the BNSTp because the number of apoptotic cells in the BNSTp between postnatal days 3 and 6 is greater in female than in male mice [41]. The sex difference in the number of apoptotic cells is inversely related to that in the number of living neurons in adulthood. Reduced estrogen levels caused by an aromatase gene deletion induce apoptotic cell death in the BNSTp of postnatal male mice [42]. We further showed that postnatal EB treatment increased the number of neurons in the BNSTp of ArKO male mice. Taking this evidence and our findings together, estrogen synthesized by aromatase during the postnatal period may protect BNSTp neurons from apoptosis. The mechanisms by which estrogen protects BNSTp neurons from apoptosis are largely unknown. However, the modulatory effects of estrogen on the expression of the Bcl-2 family, which is involved in the mitochondrial signaling pathway that regulates apoptosis, may play a role in creating the sex difference in number of neurons in BNSTp. Bax is a pro-apoptotic member of the Bcl-2 family, and in Bax-deficient mice, there is no significant sex difference in number of neurons in BNSTp in adult mice [3] or in number of apoptotic cells in BNSTp in postnatal mice [41]. Post-

natal EB treatment in female rats can reduce the degree of sex difference in the size of SDN-POA by decreasing the number of apoptotic cells [43], and this decrease is due to the up-regulation of anti-apoptotic Bcl-2 expression and the down-regulation of pro-apoptotic Bax expression in the SDN-POA of these females [44]. Therefore, estrogen may modulate the expression of the Bcl-2 family members in the BNSTp of postnatal mice. Further studies are needed to determine the exact mechanisms responsible for the effects of aromatized androgen on masculinization of the BNSTp in mice.

In summary, we showed that ArKO and αERKO male mice had smaller BNSTp volume and neuron number in the BNSTp than did their wild-type male littermates. The number of glial cells in the BNSTp of αERKO males was also lower than that of wild-type males. However, the BNSTp did not change with deletion of the ERβ gene. We further showed that postnatal EB treatment could rescue some effects of deletion of the aromatase gene on the number of BNSTp neurons. These findings suggest that masculinization of the BNSTp in mice involves the postnatal actions of estrogen that is synthesized from androgen by aromatase and that this estrogen mostly acts via ERα.

Acknowledgments

We thank K. Watai for his technical assistance. This work was supported in part by the Grants-in-Aid for Scientific Research from the Ministry of Education, Culture, Sports, Science, and Technology of Japan (No. 19681006 to S.T., No. 17330151, and No. 17052001 to S.O.), by the Project Research Grant from the Research Management Bureau of Saitama University to S.T. (A10-20), and by the University of Tsukuba Research Project, Special Research Grant to S.O.

References

1 MacLusky NJ, Naftolin F: Sexual differentiation of the central nervous system. Science 1981;211:1294–1302.
2 Morris JA, Jordan CL, Breedlove SM: Sexual differentiation of the vertebrate nervous system. Nat Neurosci 2004;7:1034–1039.
3 Forger NG, Rosen GJ, Waters EM, Jacob D, Simerly RB, de Vries GJ: Deletion of bax eliminates sex differences in the mouse forebrain. Proc Natl Acad Sci USA 2004;101:13666–13671.
4 del Abril A, Segovia S, Guillamon A: The bed nucleus of the stria terminalis in the rat: regional sex differences controlled by gonadal steroids early after birth. Brain Res 1987;429:295–300.
5 Hines M, Allen LS, Gorski RA: Sex differences in subregions of the medial nucleus of the amygdala and the bed nucleus of the stria terminalis of the rat. Brain Res 1992;579:321–326.
6 Liu YC, Salamone JD, Sachs BD: Lesions in medial preoptic area and bed nucleus of stria terminalis: Differential effects on copulatory behavior and noncontact erection in male rats. J Neurosci 1997;17:5245–5253.
7 Claro F, Segovia S, Guilamon A, Del Abril A: Lesions in the medial posterior region of the bst impair sexual behavior in sexually experienced and inexperienced male rats. Brain Res Bull 1995;36:1–10.
8 van Leeuwen FW, Caffe AR, De Vries GJ: Vasopressin cells in the bed nucleus of the stria terminalis of the rat: sex differences and the influence of androgens. Brain Res 1985;325:391–394.
9 De Vries GJ, Miller MA: Anatomy and function of extrahypothalamic vasopressin systems in the brain. Prog Brain Res 1998;119:3–20.
10 Allen LS, Gorski RA: Sex difference in the bed nucleus of the stria terminalis of the human brain. J Comp Neurol 1990;302:697–706.
11 Zhou JN, Hofman MA, Gooren LJ, Swaab DF: A sex difference in the human brain and its relation to transsexuality. Nature 1995;378:68–70.
12 Kruijver FP, Zhou JN, Pool CW, Hofman MA, Gooren LJ, Swaab DF: Male-to-female transsexuals have female neuron numbers in a limbic nucleus. J Clin Endocrinol Metab 2000;85:2034–2041.
13 Guillamon A, Segovia S, del Abril A: Early effects of gonadal steroids on the neuron number in the medial posterior region and the lateral division of the bed nucleus of the stria terminalis in the rat. Dev Brain Res 1988;44:281–290.
14 Chung WC, Swaab DF, De Vries GJ: Apoptosis during sexual differentiation of the bed nucleus of the stria terminalis in the rat brain. J Neurobiol 2000;43:234–243.
15 Durazzo A, Morris JA, Breedlove SM, Jordan CL: Effects of the testicular feminization mutation of the androgen receptor gene on bstmpm volume and morphology in rats. Neurosci Lett 2007;419:168–171.
16 Carruth LL, Reisert I, Arnold AP: Sex chromosome genes directly affect brain sexual differentiation. Nat Neurosci 2002;5:933–934.
17 De Vries GJ, Rissman EF, Simerly RB, Yang LY, Scordalakes EM, Auger CJ, Swain A, Lovell-Badge R, Burgoyne PS, Arnold AP: A model system for study of sex chromosome effects on sexually dimorphic neural and behavioral traits. J Neurosci 2002;22:9005–9014.
18 Hisasue S, Seney ML, Immerman E, Forger NG: Control of cell number in the bed nucleus of the stria terminalis of mice: Role of testosterone metabolites and estrogen receptor subtypes. J Sex Med 2010;7:1401–1409.
19 Toda K, Takeda K, Okada T, Akira S, Saibara T, Kaname T, Yamamura K, Onishi S, Shizuta Y: Targeted disruption of the aromatase p450 gene (cyp19) in mice and their ovarian and uterine responses to 17beta-oestradiol. J Endocrinol 2001;170:99–111.
20 Toda K, Okada T, Takeda K, Akira S, Saibara T, Shiraishi M, Onishi S, Shizuta Y: Oestrogen at the neonatal stage is critical for the reproductive ability of male mice as revealed by supplementation with 17beta-oestradiol to aromatase gene (cyp19) knockout mice. J Endocrinol 2001;168:455–463.
21 Lubahn DB, Moyer JS, Golding TS, Couse JF, Korach KS, Smithies O: Alteration of reproductive function but not prenatal sexual development after insertional disruption of the mouse estrogen receptor gene. Proc Natl Acad Sci USA 1993;90:11162–11166.
22 Krege JH, Hodgin JB, Couse JF, Enmark E, Warner M, Mahler JF, Sar M, Korach KS, Gustafsson JA, Smithies O: Generation and reproductive phenotypes of mice lacking estrogen receptor beta. Proc Natl Acad Sci USA 1998;95:15677–15682.
23 Toda K, Saibara T, Okada T, Onishi S, Shizuta Y: A loss of aggressive behaviour and its reinstatement by oestrogen in mice lacking the aromatase gene (cyp19). J Endocrinol 2001;168:217–220.
24 Matthews J, Celius T, Halgren R, Zacharewski T: Differential estrogen receptor binding of estrogenic substances: A species comparison. J Steroid Biochem Mol Biol 2000;74:223–234.
25 Paxinos G, Franklin KJ: The mouse brain in stereotaxic coordinates. San Diego, Academic Press, 2001.
26 Tsukahara S, Nakajima D, Kuroda Y, Hojo R, Kageyama S, Fujimaki H: Effects of maternal toluene exposure on testosterone levels in fetal rats. Toxicol Lett 2009;185:79–84.
27 Plumari L, Viglietti-Panzica C, Allieri F, Honda S, Harada N, Absil P, Balthazart J, Panzica GC: Changes in the arginine-vasopressin immunoreactive systems in male mice lacking a functional aromatase gene. J Neuroendocrinol 2002;14:971–978.
28 Ogawa S, Lubahn DB, Korach KS, Pfaff DW: Behavioral effects of estrogen receptor gene disruption in male mice. Proc Natl Acad Sci USA 1997;94:1476–1481.
29 Holmes MM, McCutcheon J, Forger NG: Sex differences in NeuN- and androgen receptor-positive cells in the bed nucleus of the stria terminalis are due to Bax-dependent cell death. Neuroscience 2009;158:1251–1256.
30 Shinoda K, Nagano M, Osawa Y: Neuronal aromatase expression in preoptic, strial, and amygdaloid regions during late prenatal and early postnatal development in the rat. J Comp Neurol 1994;343:113–129.
31 Tsuruo Y, Ishimura K, Osawa Y: Presence of estrogen receptors in aromatase-immunoreactive neurons in the mouse brain. Neurosci Lett 1995;195:49–52.
32 Tobet SA, Baum MJ: Role for prenatal estrogen in the development of masculine sexual behavior in the male ferret. Horm Behav 1987;21:419–429.
33 Tobet SA, Zahniser DJ, Baum MJ: Differentiation in male ferrets of a sexually dimorphic nucleus of the preoptic/anterior hypothalamic area requires prenatal estrogen. Neuroendocrinology 1986;44:299–308.
34 Schulz KM, Molenda-Figueira HA, Sisk CL: Back to the future: The organizational-activational hypothesis adapted to puberty and adolescence. Horm Behav 2009;55:597–604.
35 Fisher CR, Graves KH, Parlow AF, Simpson ER: Characterization of mice deficient in aromatase (arko) because of targeted disruption of the cyp19 gene. Proc Natl Acad Sci USA 1998;95:6965–6970.
36 Lindzey J, Wetsel WC, Couse JF, Stoker T, Cooper R, Korach KS: Effects of castration and chronic steroid treatments on hypothalamic gonadotropin-releasing hormone content and pituitary gonadotropins in male wild-type and estrogen receptor-alpha knockout mice. Endocrinology 1998;139:4092–4101.
37 Akingbemi BT, Ge R, Rosenfeld CS, Newton LG, Hardy DO, Catterall JF, Lubahn DB, Korach KS, Hardy MP: Estrogen receptor-alpha gene deficiency enhances androgen biosynthesis in the mouse leydig cell. Endocrinology 2003;144:84–93.
38 Couse JF, Yates MM, Rodriguez KF, Johnson JA, Poirier D, Korach KS: The intraovarian actions of estrogen receptor-alpha are necessary to repress the formation of morphological and functional leydig-like cells in the female gonad. Endocrinology 2006;147:3666–3678.
39 Couse JF, Yates MM, Walker VR, Korach KS: Characterization of the hypothalamic-pituitary-gonadal axis in estrogen receptor (ER) null mice reveals hypergonadism and endocrine sex reversal in females lacking eralpha but not erbeta. Mol Endocrinol 2003;17:1039–1053.
40 Morris JA, Jordan CL, Breedlove SM: Sexual dimorphism in neuronal number of the posterodorsal medial amygdala is independent of circulating androgens and regional volume in adult rats. J Comp Neurol 2008;506:851–859.
41 Gotsiridze T, Kang N, Jacob D, Forger NG: Development of sex differences in the principal nucleus of the bed nucleus of the stria terminalis of mice: role of bax-dependent cell death. Dev Neurobiol 2007;67:355–362.
42 Wu MV, Manoli DS, Fraser EJ, Coats JK, Tollkuhn J, Honda S, Harada N, Shah NM: Estrogen masculinizes neural pathways and sex-specific behaviors. Cell 2009;139:61–72.
43 Arai Y, Sekine Y, Murakami S: Estrogen and apoptosis in the developing sexually dimorphic preoptic area in female rats. Neurosci Res 1996;25:403–407.
44 Tsukahara S, Hojo R, Kuroda Y, Fujimaki H: Estrogen modulates bcl-2 family protein expression in the sexually dimorphic nucleus of the preoptic area of postnatal rats. Neurosci Lett 2008;432:58–63.

Early life stress disrupts peripubertal development of aggression in male mice

Mumeko C. Tsuda, Naoko Yamaguchi and Sonoko Ogawa

To investigate the effects of early life stress on the development of social behaviors in male mice, we examined behavioral responses toward same sex stimulus mice in the social investigation test and aggressive behaviors in peripubertal male mice exposed to maternal separation (MS) during the first 2 weeks of life. MS suppressed aggressive behaviors from 5–9 weeks of age, but had no effect on social investigative behaviors in the social investigation test. Investigation of neuroendocrine bases of behavioral effects of MS showed that MS reduced plasma testosterone levels and decreased arginine vasopressin and increased oxytocin immunoreactivity in the paraventricular nucleus of peripubertal males. These results collectively suggest that early life stress disrupts the development of male aggressive behaviors and associated neuroendocrine systems. *NeuroReport* **22:259–263 © 2011 Wolters Kluwer Health | Lippincott Williams & Wilkins.**

NeuroReport 2011, 22:259–263

Keywords: adolescence, maternal separation, oxytocin, paraventricular nucleus, social behavior, testosterone, vasopressin

Laboratory of Behavioral Neuroendocrinology, Graduate School of Comprehensive Human Sciences, University of Tsukuba, Tsukuba, Ibaraki, Japan

Correspondence to Sonoko Ogawa, PhD, Laboratory of Behavioral Neuroendocrinology, Graduate School of Comprehensive Human Sciences, University of Tsukuba, Research Building D-409, 1-1-1 Tennodai, Tsukuba, Ibaraki 305-8577, Japan
Tel/fax: +81 29 853 2966;
e-mail: ogawa@kansei.tsukuba.ac.jp

Received 23 November 2010 **accepted** 3 January 2011

Introduction

Adolescence is a developmental period between childhood and adulthood that involves cognitive, emotional, sexual, and social maturation [1]. Growing evidence indicates that early adverse experiences, such as childhood maltreatment, is associated with an increased risk of developing social adjustment disorders and onset of these disorders can be seen as early as the adolescent age [2,3]. Maternal separation (MS) is an animal model established to mimic the stress of early adverse experiences. In a recent study, daily MS stress during the first 2 weeks of life has been reported to modify aggressive behaviors in juvenile male rats, as indicated by increased levels of offensive play-fighting behaviors compared with control males [4]. Moreover, MS has been reported to have species-dependent consequences on male aggression in adulthood. Specifically, aggression levels were enhanced by MS in male rats [5], but reduced in male mice [6]. Thus far, the effects of MS stress on the development of social behaviors during the adolescent period have not been studied in mice. Therefore, this study examined the effects of MS on the development of aggressive behavior and behavioral responses to a same sex opponent in the social investigation test (SIT) in peripubertal male mice.

The adolescent period is generally associated with major physiological and behavioral changes triggered by testicular maturation and the production of adult levels of testosterone [7,8]. In rodents, male aggression is known to be positively correlated with circulating levels of testosterone [9] and recent studies reported that pubertal maturation of testosterone levels have organizational effects on male aggressive behaviors in adulthood [10]. To date, the effects of early life stress on pubertal development of testosterone levels remains to be determined. In mice, puberty onset has been found to occur around postnatal day (PND) 40 [11]. Therefore, we examined the effect of MS on the maturation of plasma testosterone levels from 4 weeks (before puberty) to 6 weeks (after puberty) of age in male mice.

Arginine vasopressin (AVP) and oxytocin (OT) are neuropeptides mainly synthesized in the paraventricular nucleus (PVN) and supraoptic nuclei of the hypothalamus and released peripherally through the posterior pituitary and centrally to various brain regions. Central release of both neuropeptides is reported to play a role in stress responses [12] and also in the regulation of social behaviors, including aggression [13,14]. Both AVP and OT systems are known to undergo developmental changes from the perinatal period through adulthood. Recently, MS was shown to disrupt age-dependent changes in both AVP and OT systems in the brain [4,15], which possibly contributed to enhanced levels of aggressive behaviors in juvenile and adult male rats [4,5]. However, it is still not known whether MS modifies AVP and OT systems during the peripubertal development in mice. Therefore, we investigated MS effects on AVP and OT immunoreactivity in the PVN around the peripubertal period (4–6 weeks of age).

Materials and methods

Animals and treatments

Adult C57BL/6J female and male mice (CLEA, Tokyo, Japan) were mated. Pregnant female mice were individually housed in plastic cages (29 × 19 × 12 cm) with cotton nesting material during their third week of gestation. On the day after parturition, designated as PND 1, each litter was culled to six pups (female:male ratio was as close to 1:1 as possible). MS pups were separated daily from their dam for 3 h between 15:00 h and 18:00 h from PND 1 to 14. First, MS dams were placed in a separate cage and transferred to a separate room during the separation period. Then, MS pups were placed together in a separate small container with clean bedding and kept warm at a temperature of 35°C. At 18:00 h, all pups were returned to their home-cage, immediately followed by the dam. For nonseparated (control) litters, dams and pups were handled in the same manner as MS groups, except for the separation procedure. On PND 21, all pups were weaned and group-housed with littermates of the same sex. All mice were maintained on a 12 : 12-light/dark cycle (lights off at 12:00 h) and at a constant temperature (23 ± 2°C). Food and water were provided *ad libitum*. All procedures were carried out in accordance with the National Institutes of Health guidelines and the University of Tsukuba Animal Care and Use Committee. Only male offspring were used in this study.

Behavioral testing

At 4 weeks of age, male mice from control and MS treatment groups were single-housed and assigned to one of two behavioral testing groups: (i) control ($n = 5$) and MS ($n = 7$) male mice were tested in SIT at 5 and 6 weeks of age for measurement of behavioral responses toward an unfamiliar same sex stimulus mouse and (ii) control ($n = 13$) and MS ($n = 19$) male mice were tested for aggressive behaviors from 5 to 9 weeks of age. All behavioral tests were conducted during the dark phase, 3–6 h after lights off, under red light illumination.

Social investigation test

Experimental male mice were tested in their home-cage against an unfamiliar gonadally intact C57BL/6J male mouse for 15 min. Stimulus mice were placed in clear Plexiglas cylinders (7 cm in diameter at the bottom, 5 cm in diameter at the top, 11.5 cm in height) consisting of 28 holes (6 mm in diameter) near the bottom 3 cm of the cylinder (Mouse Cylinder SIOT2, O'Hara & Co., Ltd, Tokyo, Japan) and introduced into the center of the males' home-cage. Behaviors of mice during SIT were video-recorded and cumulative duration of sniffing toward perforated parts of the cylinder (social investigation) was scored off-line using a digital event recorder program (Recordia 1.0b, O'Hara & Co., Ltd).

Aggressive behavior test

Male aggression was assessed in the resident-intruder paradigm for 3 consecutive days every week from 5 to 9 weeks of age, for a total of 15 tests. Each male was tested in his home-cage (as a resident) against a weight-matched, gonadally intact, olfactory bulbectomized C57BL/6J male intruder mouse for 15 min. Tests were video-recorded and cumulative duration of aggressive bouts in each test was scored with a digital event recorder program. Data were averaged for each week (three tests per week) for each experimental male. An aggressive bout was defined as a series of behavioral interactions consisting of at least one of the following: chasing, boxing, tail rattling, wrestling, biting, and offensive lateral attack. If the interval between two aggressive bouts exceeded 3 s, the two bouts were scored as two separate bouts.

Immunohistochemistry

A separate set of 4, 5, and 6-weeks-old control ($n = 8$ per age) and MS ($n = 8$ per age) male mice were deeply anesthetized with an intraperitoneal injection of a 1 : 1 solution containing sodium pentobarbital (60 mg/kg) and heparin (1000 units/kg) and perfused transcardially with 0.1 M phosphate buffered saline, pH 7.2, followed by 4% paraformaldehyde in 0.1 M phosphate buffer, pH 7.2. Brains were removed, postfixed in 4% paraformaldehyde in phosphate buffer, immersed in 30% sucrose in 0.1 M phosphate buffer for 48 h at 4°C, and coronally sectioned at 30 μm on a freezing microtome. Free-floating sections were incubated in (i) either anti-AVP (0.025 mg/ml; AB1565; Chemicon International Inc., Temecula, California, USA) or anti-OT (0.05 mg/ml; AB911; Chemicon International) antiserum in 0.05 M tris-buffered saline (TBS), pH 7.2, containing 1% Triton X-100, 3% normal goat serum (Vector Laboratories, Burlingame, California, USA), and 3% bovine serum albumin (Sigma-Aldrich, St. Louis, Missouri, USA) overnight at 4°C; (ii) a 1 : 250 dilution of biotinylated goat antirabbit secondary antibody (Vector Laboratories) in TBS containing 1% Triton X-100, 3% normal goat serum, and 3% bovine serum albumin for 2 h at room temperature; and (iii) the avidin–biotin complex (Vectastain ABC Elite kit, Vector Laboratories) in TBS for 1 h at room temperature. Sections were visualized with 0.03% diaminobenzidine and 0.03% hydrogen peroxide in TBS. Three anatomically matched sections for the PVN (Bregma, 0.70–0.94 mm) were selected for each animal. Images of the PVN were obtained at × 10 magnification with a digital camera mounted on an Olympus microscope and total number of immunoreactive (-ir) cells was bilaterally counted for each animal by an experimenter who was unaware of the treatment groups of the tissues.

Enzyme immunoassay for serum testosterone

For testosterone assay, serum samples were obtained from 4, 5, and 6-weeks-old control and MS male mice used for immunohistochemistry. Testosterone concentrations of serum samples were determined using a testosterone enzyme immunoassay kit (Cayman Chemicals, Ann Arbor, Michigan, USA) according to the manufacturer's protocol. The intra-assay standard variation was 8.7% and the interassay coefficient of variation was 10.3%.

0959-4965 © 2011 Wolters Kluwer Health | Lippincott Williams & Wilkins

DOI: 10.1097/WNR.0b013e328344495a

Statistics

Data were analyzed by a two-way analysis of variance (ANOVA) for repeated measurements (SIT and aggression data) or independent measurements (immunohistochemical and hormonal data) for the main effects of treatment, age, and their interactions. Differences in the percentages of animals that exhibited aggression were analyzed with a χ^2 test and differences in the average number of weeks mice showed aggression out of 5 weeks of testing were analyzed by *t*-tests. All data are presented as mean ± standard error of the mean. When appropriate, ANOVAs were followed by Bonferroni post-hoc test. Significant differences were considered when *P* value was less than 0.05.

Results

Social investigation

Social behavioral responses toward an unfamiliar same sex stimulus mouse were not altered by MS stress in 5 weeks and 6-weeks-old male mice. Control and MS male mice exhibited similar levels of social sniffing toward the stimulus mouse at both ages (Fig. 1a).

Aggressive behavior

MS greatly modified aggression levels of peripubertal male mice, as indicated by significant main effects of treatment and age on cumulative duration of aggression [(treatment: $F(1,30) = 9.45$, $P < 0.01$; age: $F(4,120) = 6.84$, $P < 0.0001$; treatment × age: not significant); Fig. 1b]. Post-hoc analysis showed that compared with 5 weeks, control male mice began to exhibit higher levels of aggression from 6 weeks of age and continued to be aggressive for the following weeks. In contrast, MS male mice displayed very little increase from 5 weeks of age and consistently showed significantly lower levels of aggression throughout all ages compared with control male mice. Moreover, number of male mice that displayed aggression increased with age in control male mice [5 vs. 8 weeks: $\chi^2(1) = 6.50$, $P < 0.05$; 5 vs. 9 weeks: $\chi^2(1) = 7.08$, $P < 0.05$], in which by 9 weeks of age, 92% of mice showed aggression; however, no such increase was seen in MS male mice (Table 1). Therefore, from 7 weeks of age, significantly less MS males exhibited aggression compared to control male mice [7 weeks: $\chi^2(1) = 4.39$, $P < 0.05$; 8 weeks: $\chi^2(1) = 11.57$, $P < 0.01$; 9 weeks: $\chi^2(1) = 6.91$, $P < 0.01$]. Furthermore, average number of weeks MS male mice displayed aggression out of 5 weeks of testing was significantly less compared with control mice [$t(30) = 3.72$, $P < 0.001$); Table 1].

Fig. 1

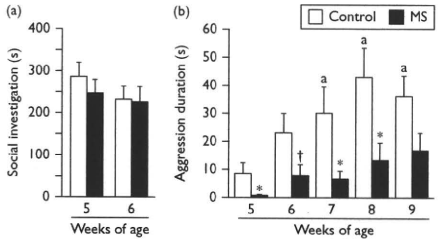

Effects of maternal separation (MS) on social investigation duration in (a) social investigation test and (b) cumulative duration of aggression in peripubertal male mice. All data are presented as mean ± standard error of the mean. †$P < 0.1$ and *$P < 0.05$ versus control of same age; [a]$P < 0.05$ versus 5 weeks of age in the same treatment group.

Serum testosterone levels

Out of 48 samples measured for serum testosterone levels, five samples did not yield detectable levels and were therefore discarded from further analysis. Two-way ANOVAs of the remaining samples showed that MS greatly reduced serum testosterone levels compared with control male mice [$F(1,37) = 9.09$, $P < 0.01$; Fig. 2a]. Furthermore, serum testosterone levels in control male mice significantly increased with age, whereas no such age-dependent changes were found in MS male mice [age: $F(2,37) = 5.82$, $P < 0.01$; age × treatment: $F(2,37) = 3.80$, $P < 0.05$].

Oxytocin immunoreactivity in the paraventricular nucleus

There was a significant main effect of MS on the number of OT immunopositive cells in the PVN [($F(1,42) = 7.85$, $P < 0.01$); Fig. 2b], but no effect of age or interaction. Further analysis showed that MS male mice had a higher number of OT positive cells at 4 weeks ($P < 0.05$) and 6 weeks ($P < 0.05$; Fig. 2d and e) of age compared with control male mice.

Arginine vasopressin immunoreactivity in the paraventricular nucleus

An MS effect on the number of AVP positive cells in the PVN was found [($F(1,42) = 16.57$, $P < 0.01$); Fig. 2c], but there was no effect of age or interaction.

Table 1 Number and percentage of mice that showed aggression in at least one test each week and average number of weeks male mice exhibited aggression

	Control ($n = 13$)	MS ($n = 19$)
Age (weeks)		
5	6/13 (46.2%)[a]	4/19 (21.1%)
6	7/13 (53.8%)	6/19 (31.6%)
7	10/13 (76.9%)	6/19 (31.6%)*
8	12/13 (92.3%)†	6/19 (31.6%)**
9	12/13 (92.3%)†	9/19 (47.4%)**
Average number of weeks showed aggression	3.7 ± 0.4[b]	1.6 ± 0.3*

[a]Number of mice that showed aggression/total number of mice tested, percentage of mice that showed aggression (in parentheses).
[b]Average number of weeks showed aggression out of 5 weeks of testing.
*$P < 0.05$ versus control.
**$P < 0.01$ versus control.
†$P < 0.05$ versus 5 weeks of age.

Fig. 2

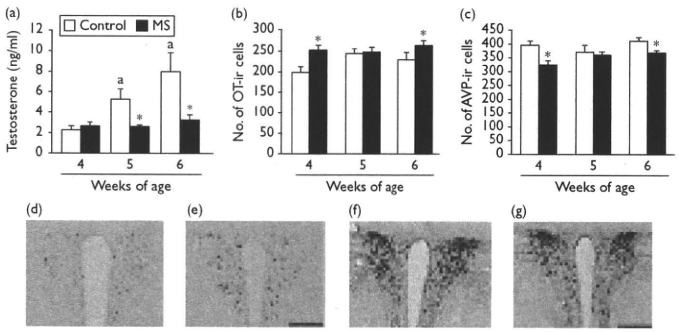

(a) Maternal separation (MS) effects on plasma testosterone levels and (b) number of oxytocin (OT) and (c) arginine vasopressin (AVP) immunopositive cells in the paraventricular nucleus (PVN) of peripubertal male mice. Representative photomicrographs of OT immunopositive cells of (d) control and (e) MS male mice and AVP immunopositive cells of (f) control and (g) MS male mice in the PVN at 6 weeks of age. The scale bar represents 200 μm. All data are presented as mean ± standard error of the mean. *$P < 0.05$ versus control in the same age group; [a]$P < 0.05$ versus 4 weeks of age in the same treatment group. ir, immunoreactive.

Subsequent post-hoc analysis showed that MS reduced the number of AVP immunopositive cells in 4 weeks ($P < 0.05$) and 6-weeks-old male mice ($P < 0.05$; Fig. 2f and g).

Discussion

In this study, we provide new evidence that neonatal MS stress may specifically disrupt the pubertal development of male aggressive behaviors, as indicated by reduced levels of aggression, but no MS effects on social investigative behaviors toward a same sex opponent in SIT during the peripubertal period. Furthermore, our results showed that unlike control male mice, MS male mice failed to show a significant increase of aggression with age, suggesting the possibility of a delayed or inhibited pubertal onset of aggression. In rodents, adolescence is considered to last from approximately PND 21 to PND 60 [11] and onset of agonistic and aggressive behaviors during this period is essential for the further development of adequate adult social behaviors [16]. In an earlier study, MS was reported to decrease levels of aggressive behaviors in male mice subjected to MS stress during the first 2 weeks of life when tested in adulthood [6]. Taken together, these results suggest that MS-induced disruption of the development of pubertal aggressive behaviors may have led to reduced aggression levels found in adult MS male mice.

Onset of puberty in rodents is considered to occur around PND 40 [11] and it is known that there is a pubertal maturation of testosterone levels at this time [1,7,8]. Studies that investigated the effect of prenatal stress on the onset of puberty in male rats and mice reported no significant disruptions in the timing of puberty onset, as measured by luteinizing hormone secretion and balanopreputial gland separation [17,18]. In contrast, our results showed that plasma testosterone levels were significantly lower in peripubertal MS male mice and these male mice also failed to exhibit an increase in testosterone levels at 5 weeks of age as seen in control male mice. As we found that body weight of peripubertal MS male mice did not differ from control male mice (unpublished observation), low testosterone levels did not necessarily affect the physical development of MS male mice. However, it is still possible that neonatal MS stress may disrupt the timing of puberty onset through alterations in testosterone levels in male mice. Furthermore, plasma testosterone levels are known to be positively correlated with male aggression levels in most rodents [9]. Therefore, reduced levels of plasma testosterone in MS male mice might be partly involved in reduced aggressive behaviors found in this study.

In this study, we found that MS treatment decreased the number of AVP and increased the number of OT immunopositive cells in the PVN compared with control male mice. Central release of AVP and OT from PVN neurons to other hypothalamic and limbic brain regions play an important role in the regulation of social behaviors such as male aggression [19,20]. Furthermore, AVP and OT are known to often exert an opposite action in the regulation of male aggression, in which AVP can facilitate and OT can inhibit the levels of aggression [13]. In this respect, MS-induced changes in AVP and OT activity in opposing directions corroborates the suppressed levels of aggressive behaviors in peripubertal MS male mice. It should be noted that MS effects on the number of AVP

Behavioural Brain Research 221 (2011) 172–181

Contents lists available at ScienceDirect

Behavioural Brain Research

journal homepage: www.elsevier.com/locate/bbr

Research report

Automated test of behavioral flexibility in mice using a behavioral sequencing task in IntelliCage

Toshihiro Endo[a], Fumihiko Maekawa[c], Vootele Võikar[d], Asahi Haijima[a], Yukari Uemura[b], Yan Zhang[a], Wataru Miyazaki[a], Shigetomo Suyama[c], Kuniko Shimazaki[c], David P. Wolfer[e,f], Toshihiko Yada[c], Chiharu Tohyama[a], Hans-Peter Lipp[d], Masaki Kakeyama[a,*]

[a] Laboratory of Environmental Health Sciences, Center for Disease Biology and Integrative Medicine, Graduate School of Medicine, The University of Tokyo, Japan
[b] Department of Biostatistics, School of Public Health, The University of Tokyo, Japan
[c] Department of Physiology, Division of Integrative Physiology, Jichi Medical University, School of Medicine, Japan
[d] Institute of Anatomy, University of Zurich, Switzerland
[e] Institute of Anatomy and Zurich Center for Integrative Human Physiology, University of Zurich, Switzerland
[f] Institute of Human Movement Sciences, ETH Zurich, Switzerland

ARTICLE INFO

Article history:
Received 6 September 2010
Received in revised form 23 February 2011
Accepted 28 February 2011

Keywords:
Mouse
Automated analysis
Serial reversal learning
Behavioral flexibility
IntelliCage

ABSTRACT

There has been a long-standing need to develop efficient and standardized behavioral test methods for evaluating higher-order brain functions in mice. Here, we developed and validated a behavioral flexibility test in mice using IntelliCage, a fully automated behavioral analysis system for mice in a group-housed environment. We first developed a "behavioral sequencing task" in the IntelliCage that enables us to assess the learning ability of place discrimination and behavioral sequence for reward acquisition. In the serial reversal learning using the task, the discriminated spatial patterns of the rewarded and never-rewarded places were serially reversed, and thus, mice were accordingly expected to realign the previously acquired behavioral sequence. In general, the tested mice showed rapid acquisition of the behavioral sequencing task and behavioral flexibility in the subsequent serial reversal stages both in intra- and inter-session analyses. It was found that essentially the same results were obtained among three different laboratories, which confirm the high stability of the present test protocol in different strains of mice (C57BL/6, DBA/2, and ICR). In particular, the most trained cohort of C57BL/6 mice achieved a markedly rapid adaptation to the reversal task in the final phase of the long-term serial reversal test, which possibly indicated that the mice adapted to the "reversal rule" itself. In conclusion, the newly developed behavioral test was shown to be a valid assay of behavioral flexibility in mice, and is expected to be utilized in tests of mouse models of cognitive deficits.

1. Introduction

The behavioral characterization of genetically modified mice as well as wild-type strains has become a powerful tool for investigating not only the molecular bases of normal brain functions but also the pathogenesis and treatment of neuropsychological disorders [1–9]. However, the levels of efficiency, standardization, and reproducibility of the testing methods for mouse behavioral assessment have been considered still inadequate [10–14]. More importantly, the limited number of established "higher-order" cognitive test paradigm for mice makes it difficult for researchers to determine the accurate neurobehavioral phenotypes of both wild-type and pathological mice [15].

To overcome this problem, a number of computer-assisted technologies for automatically capturing rodent behavior over long periods have become available [16–18]. Among them, IntelliCage (New Behavior AG; http://www.newbehavior.com/) used in the present study is a unique approach in the sense that this system is specially designed for the cognitive assessment of group-housed mice. The IntelliCage system can be a powerful tool for the behavioral characterization of mice by at least fivefold. First, its use makes it possible to achieve a sensitive and highly standardized experiment by minimizing the artifacts that arise from unavoidable differences among experimenters or other laboratory-specific conditions. Second, long term monitoring of mouse behavior can be performed in a familiar and thus less stressful environment. Third, high-throughput testing is possible by analyzing a maximum of 16 mice simultaneously. Fourth, experimenters can design and use their own original cognitive task depending on their research objective. Fifth, IntelliCage can be run in a fully automated manner,

* Corresponding author. Tel.: +81 3 5841 1415; fax: +81 3 5841 1434.
E-mail address: kake@m.u-tokyo.ac.jp (M. Kakeyama).

0166-4328/$ – see front matter © 2011 Elsevier B.V. All rights reserved.
doi:10.1016/j.bbr.2011.02.037

utilizing sensors and four operant conditioning units placed in each corner of the cage.

Recent studies have already shown the advantages of using this IntelliCage system in the spontaneous and learning behavioral analysis of mice [19–27]. By contrast, there are still few established protocols for IntelliCage that focus on higher-order cognitive skills typified by executive brain functions. The executive brain function is a shorthand description of a set of cognitive processes that are responsible for appropriately organizing, performing, and maintaining goal-directed actions under ever-changing environmental contexts [28–32]. The quality of life based on intellectual and mental integrity is largely dependent on such brain function, and its dysfunction is widely seen in people with aging-associated cognitive decline and various neuropsychological disorders [29,33–37] as well as patients with frontal lobe damage caused by traumatic brain injury and cerebrovascular disease [38,39]. Although researchers have recently established executive function tests for mice such as attentional set-shifting task [40–43] and selective attention [44], few reports that assessed the executive functions of group-housed mice in a computerized, high-throughput manner are available.

Thus, the aim of this study is to establish a behavioral test protocol for mice that enables one to evaluate behavioral flexibility as one of the executive brain functions using IntelliCage. The test is composed of a newly developed "behavioral sequencing task" followed by its serial reversals. The test paradigm was originally developed on the basis of the idea of the Brixton Spatial Anticipation Task [45] which has been utilized as one of the clinical assessment methods of human executive functions using a visuospatial sequencing task [45–52]. By using the IntelliCage-based test in this study, it became possible to address not only acquisition of spatial and temporal pattern of rewarded places but also behavioral flexibility of mice in various time scales in a fully automated manner. The reproducibility of the protocol was verified by different experimenters at three different laboratories located in the University of Tokyo (UT), Tokyo Japan, Jichi Medical University (JMU), Tochigi, Japan and the University of Zurich (UZH), Zurich, Switzerland, using three strains of mice (C57BL/6, DBA/2 and ICR) and of different ages (from 2 to 8 months old).

2. Materials and methods

2.1. Animals and facilities

The experiments described in this study were conducted using identical type of IntelliCage systems at three different laboratories located at the University of Tokyo (UT), Tokyo, Japan, Jichi Medical University (JMU), Tochigi, Japan and the University of Zurich (UZH), Zurich, Switzerland. All the animal experiments were performed in a humane manner in accordance with the local guidelines of each institution.

At UT, male C57BL/6 (B6-UT, 6 months old, $n=8$) and DBA/2 (D2-UT, 8 months old, $n=8$) mice were used. All mice were purchased from CLEA Japan (Tokyo, Japan) and housed in 22 ± 1 °C, $50\pm10\%$ humidity, 12 h LD cycle (lights on 8:00–20:00). At JMU, male C57BL/6 (B6-JMU, 3 months old, $n=15$) and ICR mice (ICR-JMU, 2 months old, $n=11$) were used. All mice were purchased from CLEA Japan and Japan SLC, Inc. (Shizuoka, Japan) and housed in 22 ± 1 °C, $60\pm10\%$ humidity, 12 h LD cycle (lights on 7:00–19:00). At UZH, young (3 months old) and aged (12 months old) male mice of C57BL/6 and DBA/2 strains were used (Young B6-UZH, Aged B6-UZH, Young D2-UZH and Aged D2-UZH, $n=11$, 12, 12 and 11, respectively). All mice were purchased from Charles-River Laboratories (Sulzfeld, Germany) and housed in 21 ± 1 °C, $50\pm5\%$ humidity, 12 h LD cycle (lights on 20:00–8:00 as reversed cycle). In total, eight cohorts of male mice were analyzed using the IntelliCage system as described below.

All the animals were subcutaneously implanted with a glass-covered transponder with unique ID codes (Datamars SA) for radio-frequency identification (RFID)-based animal identification before the start of the experiments under light-anesthesia with diethyl ether or isoflurane.

2.2. IntelliCage apparatus

IntelliCage (NewBehavior AG; http://www.newbehavior.com) is a computer-based, fully automated testing apparatus used to analyze the spontaneous and learning behavior of RFID-tagged mice in a home cage (Fig. 1A). (For further descriptions, see [19–27]). In short, a large standard plastic cage ($55\times37.5\times20.5\,cm^3$) equipped with four triangular operant learning chambers (corners, hereafter) ($15\times15\times21\,cm^3$) that fit into each corner of the cage, RFID readers, and other types of sensor allows simultaneous monitoring of up to 16 transponder-tagged mice living in the same cage. Mice were allowed to enter the corner (corner visit, hereafter) through a short narrow tunnel that functions as an RFID antenna. In this unit, only one mouse can enter a corner at a time because of the limited size of the corner and tunnel. In the inner space of the corner, mice can find two nosepoke holes with an infrared beam-break response detector. The "correct" nosepoke triggers the opening of a motorized access gate to water-bottle nipples (gate, hereafter). In IntelliCage, the time and duration of each behavioral event (corner visit, nosepoke and lick), mouse ID and corner ID were automatically recorded through RFID readers, infrared sensors and lickometers.

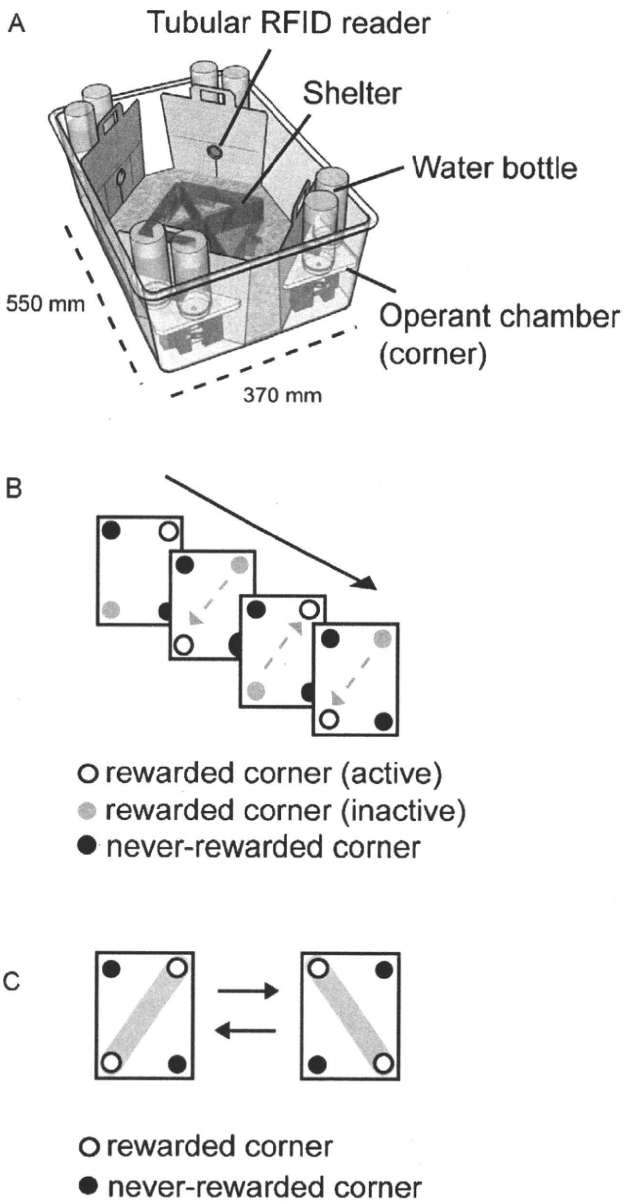

Fig. 1. Apparatus and task paradigm. (A) Overview of IntelliCage apparatus. Mice were group-housed and their behavioral responses (corner visits, nosepokes, and lickings) were monitored in a fully automated manner. The tubular RFID reader can record an implanted ID number when a mouse visits a corner where it can receive water as a reward. (B) Diagrams of behavioral sequencing task. Mice obtained a reward by alternately visiting the two distantly positioned rewarded corners (open circle). A visit to the never-rewarded corners (black circles) was counted as an "error" choice. (C) Serial reversal learning of the behavioral sequencing task. The patterns of corner conditions (rewarded or never-rewarded) were reversely switched every several sessions. The thick grey line in (C) indicates the expected shuttling path on which mice shuttle between the distantly positioned rewarded corners.

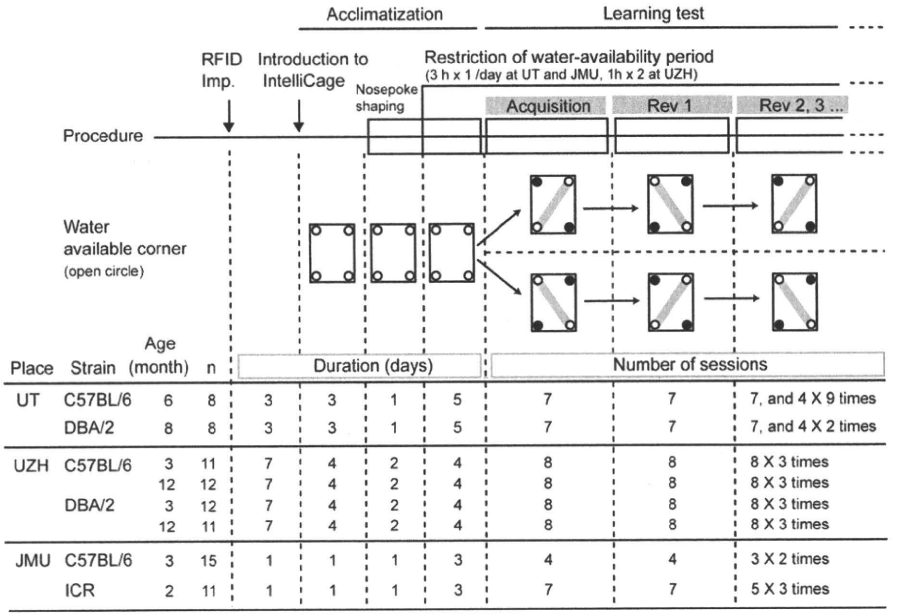

Place	Strain	Age (month)	n	Duration (days)				Number of sessions		
UT	C57BL/6	6	8	3	3	1	5	7	7	7, and 4 X 9 times
	DBA/2	8	8	3	3	1	5	7	7	7, and 4 X 2 times
UZH	C57BL/6	3	11	7	4	2	4	8	8	8 X 3 times
		12	12	7	4	2	4	8	8	8 X 3 times
	DBA/2	3	12	7	4	2	4	8	8	8 X 3 times
		12	11	7	4	2	4	8	8	8 X 3 times
JMU	C57BL/6	3	15	1	1	1	3	4	4	3 X 2 times
	ICR	2	11	1	1	1	3	7	7	5 X 3 times

Fig. 2. Overview of experimental procedures in the three laboratories (UT, JMU, and UZH). After RFID implantation and introduction to the IntelliCage, mice were habituated to the apparatus and water restriction period for 5–10 days and subsequently imposed with a learning test. Note that there are some modifications in terms of the duration of acclimatization period and number of sessions in the learning test in each laboratory.

2.3. Test protocols

We used an identical learning test protocol among the three laboratories except for small modifications such as schedule of acclimatization and number and time of sessions. The program was originally developed at UT, and provided to JMU and UZH where the program was used with minor modifications of experimental procedure (Fig. 2).

2.3.1. Acclimatization

We accommodated mice of the same age and strain in each IntelliCage at the three laboratories. In detail, groups named B6-UT (12), D2-UT (12), Young B6-UZH (11), Aged B6-UZH (12), Young D2-UZH (12), Aged D2-UZH (11), B6-JMU (15), and ICR-JMU (11) had the number of mice per cage as shown in parentheses. In order to adjust the number of mice per cage of B6-UT ($n = 8$) and D2-UT ($n = 8$) close enough to the other cohorts, additional mice were put to each cage and tested in the same manner. Although the additional mice were same in age and strain as those of mice in each cohort, their behavioral data were excluded from the analysis because they had different histories of developmental condition for the sake of another experiment. The gates through which mice can have access to water-bottle nipples in all corners were kept opened, and thus, the mice were allowed to have water *ad libitum* in each corner for the first three days (UT) of the acclimatization phase. Next, shaping of nosepoking behavior was performed for a total of six days (UT). In this phase, all the gates in front of the water bottles were closed initially so that mice had to nosepoke to open the gate and drink the water. The gate could be opened only by the first nosepoke in one corner visit, and was closed after 4 s. During the first day, mice obtained water by nosepokes at any time during the 24 h. Afterwards, nosepokes did not open the gates except during a 3 h period from 22:00 to 1:00 (UT) (i.e., all the mice were deprived of water outside these hours). During this 3 h period, a blue light-emitting diode (LED), which was attached to the outside of the cage, was dimly lighted to signal the water-availability period at UT. Likewise, during this period, red LEDs in the corner were lighted when mice made a visit. During acclimatization, all the mice visited all the four corners extensively. Their individual corner preferences varied between 20% and 30% (chance level 25%), indicating that all the mice became familiar with all the corners without any intensive preference for specific corner(s).

2.3.2. Behavioral sequencing task

After acclimatization, a behavioral sequencing task was imposed on the animals. This task, which was programmed using the graphic task designer software of the IntelliCage system, was imposed on mice and valid only during a 3 h period (UT) within a day (22:00–1:00). Thus, all the mice were deprived of water outside these hours in the same manner as in the last acclimatization phase. In the behavioral sequencing task (Fig. 1B), mice were imposed to discriminate the rewarded and never-rewarded corners, and to "shuttle" between the two distantly positioned rewarded corners. Each mouse could open the gate and drink water for 4 s only from the corners designated as "rewarded", while they could not do so in the "never-rewarded" corners. Additionally, each of the two distantly positioned rewarded corners had two distinct states, "active" or "inactive", in a mutually exclusive manner between them. That is, there is always one "active" rewarded corner, one "inactive" rewarded corner, and two never-rewarded corners at a time. The gates could be opened by a nosepoke action only in an "active" rewarded corner. When a mouse did a nosepoke in the "active" rewarded corner, and was presented a reward, the corner became "inactive". At the same time, the other rewarded corner, which was previously "inactive", became "active". This event-related alternation of the corner assignment was controlled for each mouse separately by IntelliCage software which ran throughout the experiment. Thus, the mice could not receive an additional reward by staying at one corner or by re-entering the same corner. Consequently, the mice had to shuttle between the two distantly positioned rewarded corners, avoiding temptations of entering the neighboring never-rewarded corners or just re-entering a specific corner. All the corner assignments were balanced within a group in the cage so that no specific corner would receive more traffic than others. As an "acquisition" stage, this behavioral sequencing task lasted for seven sessions in all the UT experiments, four sessions in a B6-JMU experiment, seven sessions in an ICR-JMU experiment, and eight sessions in all UZH experiments (Fig. 2). At UZH, the protocol had to be modified allowing 2 sessions per day (11:00–12:00 and 16:00–17:00), because the animal welfare guidelines at UZH did not allow water deprivation for more than 18 h.

2.3.3. Serial reversal learning

Subsequently, serial reversal task using the behavioral sequencing task paradigm were imposed on mice: Diagonal spatial patterns of rewarded and never-rewarded corners were reversely changed repetitively every 4–7 sessions. Thus, the mice had to learn to switch their shuttling behavior between the two diagonal spatial patterns (Fig. 1C). In total, 57 sessions, one session per day, were conducted in the UT experiment including the first seven sessions as an acquisition phase and further sessions with 11 serial reversals. At JMU, a total of 14 and 29 sessions, including 3 and 4 serial reversals, respectively, were carried out for B6-JMU and ICR-JMU, respectively, with one session per day. At UZH, a total of 40 sessions, including 4 serial reversals, were carried out with two sessions per day.

2.4. Behavioral scores

Corner visit of mice was defined as entering a corner chamber regardless of a nosepoke action. The records during each session were used to calculate the following four types of learning score: (1) Discrimination error rate = percentage of incorrectly visiting the two never-rewarded corners within the first 100 visits in each session; (2) Alternation score = percentage of alternate visits in specific diagonals (rewarded or never-rewarded) within total visits in a session or choice block (see Fig. 3, Fig. 7B and Supplemental Fig. S3); (3) Cumulative errors = a cumulative number of corner visits to never-rewarded corners; (4) Discrimination index = [10 − (number of errors within 10 choices) × 10]. This index was used to analyze the dynamics of within-session adaptation to the reversal learning.

2.5. Statistical analyses

All statistical analyses for possible difference in means in behavioral scores were carried out using SAS software (SAS Institute Inc.). In ANOVA, repeated

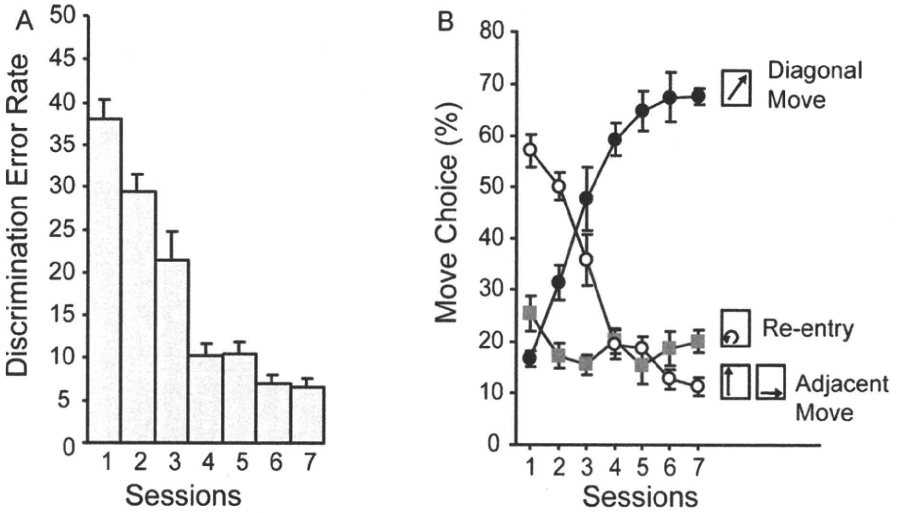

Fig. 3. Acquisition of behavioral sequencing task in B6-UT. (A) Reduction of visits to never-rewarded corners (errors) in the acquisition phase (sessions 1–7) in behavioral sequencing task. Discrimination error rate (mean ± S.E.M, $n = 8$) was defined as the number of visits to the two never-rewarded corners within the first 100 visits in each session, which makes the chance value of discrimination error rate 50%. Statistical analysis showed significant linear trends of error reduction ($p < 0.05$, one-way repeated measures ANOVA with session as a factor). See also Supplemental Fig. S2 for the other cohorts. (B) Acquisition of "shuttling" behavior in behavioral sequencing task. Three move choices in two consecutive corner visits were classified as follows: (1) diagonal move, (2) adjacent move (move to either of two adjacent corners), and (3) re-entry to the same corner, and thus chance values are calculated as 25%, 50%, and 25%, respectively. The rates of the three choices of move in the acquisition phase are shown (mean ± S.E.M, $n = 8$). The concurrent increase in diagonal move choice rate and the decrease in adjacent move choice rate indicated that the mice in this experiment acquired shuttling behavior.

analysis using a session or block of responses as a factor was adopted to assess a within-subject effect of training throughout sessions. Multiple comparisons were performed with Dunnett's test. For logarithmic curve fitting and R^2 value calculation, Excel (Microsoft) was used.

3. Results

3.1. Acquisition of behavioral sequencing task

In the behavioral sequencing task, the mice were imposed to discriminate rewarded from never-rewarded corners with attainment of shuttling behavior between the two distantly positioned rewarded corners to obtain water continuously (Fig. 1B). The discrimination error rate, defined as the number of incorrectly visiting the two never-rewarded corners within the first 100 visits in each session, was significantly decreased in C57BL/6 mice examined at the UT (B6-UT), which is the representative cohort of the present study (Fig. 3A) ($F = 49.77$, df = 6/49, $p < 0.0001$, repeated measures ANOVA). A significant decrease in discrimination error rates occurred from sessions 2 to 4 (ANOVA, Dunnett, $p < 0.001$), followed by its drop to less than 10% during sessions 6 and 7. To analyze the attainment of shuttling behavior, three move choices in two consecutive corner visits were classified as follows: (1) diagonal move, (2) adjacent move (move to either of two adjacent corners), and (3) re-entry to the same corner, and thus chance values are calculated as 25%, 50%, and 25%, respectively. The rates of the three move choices in the acquisition phase of B6-UT are representatively shown in Fig. 3B. The concurrent increase in diagonal move choice rate and the decrease in adjacent move choice rate indicated that the mice in this experiment acquired the shuttling behavior between the diagonally positioned corners. The alternation score (percentage of alternate visits in each rewarded and never-rewarded diagonal) within a session are shown in Supplemental Fig. S3A (session 1) and S3B (session 7) and indicates that the mice showed shuttling specifically in a rewarded diagonal through the session 7. As the once acquired shuttling behavior had been kept at a high level through the subsequent sessions, we will focus on discrimination error rate as an index of behavioral flexibility in the following part in this article.

We found that all the other cohorts of mice, comprising different strains and ages used at the three independent laboratories, showed almost identical learning curves of discrimination error rates, with statistically significant linear trends of error reduction ($p < 0.05$, one-way repeated measures ANOVA with session as a factor) (see Supplemental Fig. S2). Although the reduction of errors varied according to strain, age and laboratory during the first three sessions, mice of all the cohorts showed a highly significant reduction in errors after session 4. It is notable that all the cohorts of mice robustly showed a "stepwise" acquisition of place discrimination in this task.

Throughout the experiments, we had the cages including the corners cleaned routinely once a week in the middle of the acquisition phase and the subsequent test phase, and did not find significant effects of the cleaning on the task performance. For information about a probe trial supplementarily conducted at UT, see Supplemental Fig.S1 and the legend.

3.2. Serial reversal learning

In serial reversal learning using the behavioral sequencing task paradigm, diagonal spatial patterns of rewarded and never-rewarded corners were reversely changed every 4 to 7 sessions (B6-UT). Thus, the mice were anticipated to switch their shuttling behavioral sequence between the two diagonals (Fig. 1C). We first analyzed the discrimination error rates for each session to clarify the inter-session dynamics of behavioral flexibility. The discrimination error rates of the three cohorts of C57BL/6 mice in the three laboratories are representatively shown in Fig. 4. In comparison with the last session of the acquisition phase and the first session of the first reversal stage (Rev 1), the discrimination error rate of all the three cohorts was found to be markedly increased to approximately 60% each, exceeding the chance level (=50%) in each cohort (see sessions 8, 9, and 5 of Fig. 4A–C, respectively). Subsequently, those cohorts displayed a significant reduction in the discrimination error rate during the following several sessions within Rev 1, showing inter-session enhancement of behavioral flexibility. This learning curve could be robustly found in all the subsequent reversal stages in each cohort (Rev 2 and later). It is also notable that

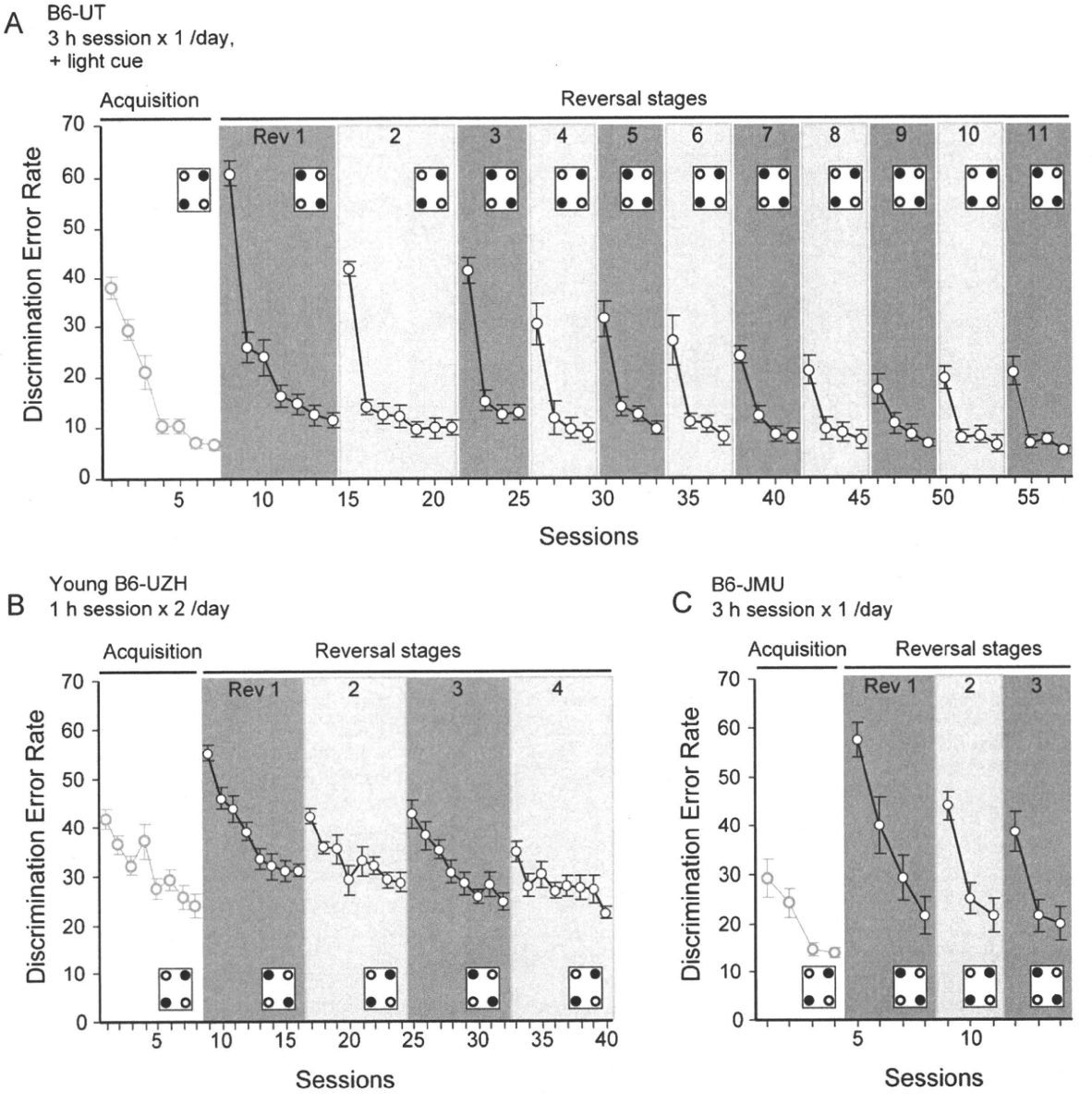

Fig. 4. Behavioral flexibility in serial reversal learning. Representative data on discrimination error rates (mean ± S.E.M) of C57BL/6 cohorts at (A) UT ($n = 8$), (B) UZH (young cohort, $n = 11$) and (C) JMU ($n = 15$) are shown. After the acquisition of place discrimination in the behavioral sequencing task, the patterns of corner conditions (rewarded or never-rewarded) were reversely changed repetitively every several sessions (reversal stages) as described in the figure. In the first session of each reversal stage (Rev), discrimination error rate transiently increased and gradually decreased within the following several sessions, indicating the dynamics of behavioral flexibility to the altered contingency.

a continued reduction of the discrimination error rate in the first sessions of each reversal stage (Rev) was observed in each cohort, which will be discussed in detail later as inter-reversal stage (Rev) improvement of behavioral flexibility.

We next analyzed the intra-session performance in detail. Fig. 5A representatively shows cumulative errors plotted for the first 100 visits in specific sessions in B6-UT mice. We found that the cumulative errors increase linearly in sessions 1 and 7 (the first and last sessions of the acquisition phase, respectively), and session 8 (the first session of Rev 1). In contrast, at session 15 (the first session of Rev 2), cumulative errors in the first half of the session exceeded the chance value (broken line), but then fell to below the chance value in the second half. This suggested that the mice realigned their behavior to the altered contingency rapidly within a session. The alternation scores (percentage of alternate visits) for both rewarded and never-rewarded diagonals also revealed a trinitarian process of the mice shifting the shuttling behavior in session 15 (Supplemental Fig. S3D), that is, the periods of (1) exceeded preference to the shuttling between the never-rewarded corners (from 0 to 15 choices), (2) similar preference between the correct and incorrect shuttling (from 20 to 45 choices), and (3) exceeded preference to the rewarded corners of mice. Since the x-axis of intra-session analyses is considered to reflect essentially a time, the time course of transition of mice responses, that is, an intra-session dynamics of behavioral flexibility can be observed. Subsequently, we plotted the discrimination index of the first sessions in different reversal stages (Revs 1, 3, 5, 7, and 9) to observe both short term and long term dynamics of behavioral flexibility (Fig. 5B). We found that logarithmic curves can be fitted well to each intra-session learning curve after Rev 3 ($R^2 = 0.835$–0.940), indicating that the reshaping of behavior mainly occurred in the early phase of each session. In addition, the step-by-step enhancement of the general adaptability was confirmed as mice proceeded to experience sequential reversal stages.

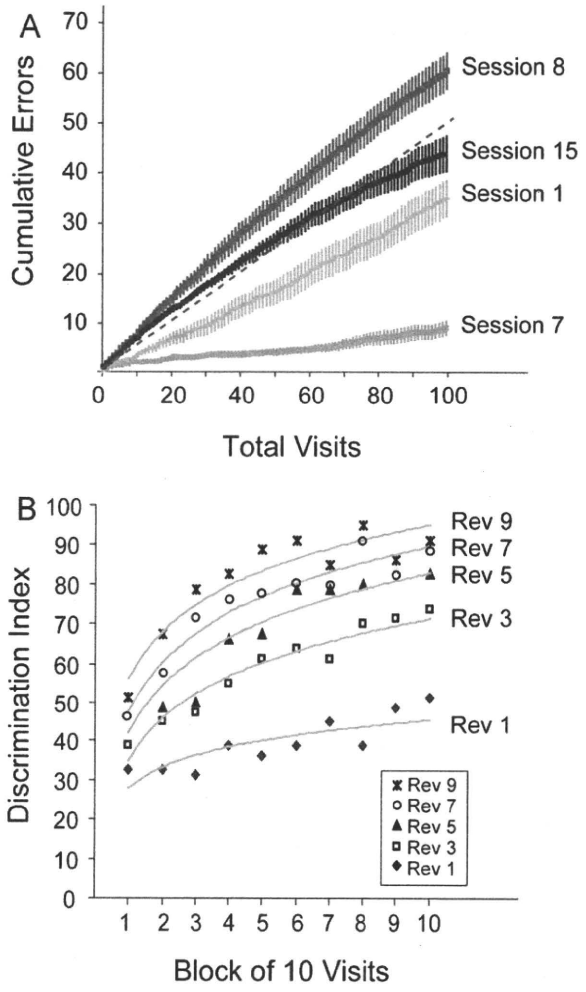

Fig. 5. Intra-session dynamics of behavioral flexibility in B6-UT mice. (A) Cumulative errors (mean ± S.E.M, $n = 8$) of the first 100 visits in sessions 1 and 7 (the first and last sessions of acquisition phase, respectively), and sessions 8 and 15 (the first sessions of Revs 1 and 2, respectively). The dotted line indicates a chance value (50 cumulative errors per 100 visits). (B) Means of discrimination index [10 − (number of errors within 10 visits) × 10] in the first sessions of Revs 1, 3, 5, 7, and 9 were plotted (mean ± S.E.M, $n = 8$). The logarithmic transformation was used for curve fitting to show the increased discrimination performance in the first sessions of Revs 1, 3, 5, 7, and 9 with reliable R^2 values (0.876, 0.939, 0.835, 0.940, and 0.651, respectively).

Lastly, we noted the fact that the mice progressively improved their behavioral flexibility performance in the serial reversals. So we directly compared the discrimination error rates in the first, second, third, and fourth sessions of the different reversal stages (Revs) (Fig. 6). In all the eight cohorts of mice, the discriminative performance consistently improved among the reversal stages (Revs), particularly in the first sessions with a significant linear trend of error reduction ($p < 0.05$, repeated measures ANOVA). In B6-UT mice, which were the most trained cohort in our study, this inter-reversal stage (Rev) improvement of behavioral flexibility finally resulted in a markedly rapid adaptation to the reversed contingency (Fig. 7A) and rapid reshaping of shuttling behavior (Fig. 7B and Supplemental Fig. S4).

4. Discussion

The significant outcome of the present study is that we established a fully automated behavioral test protocol for mice using IntelliCage to assess the acquisition of spatial and temporal patterns of rewarded place and behavioral flexibility as one of the modules of executive brain functions in mice. This test consists of a behavioral sequencing task followed by its serial reversals, which was originally developed based on the idea of Brixton Spatial Anticipation Task [45] which has been utilized as one of the clinical assessment methods of human executive functions using a visuospatial sequencing task [45–52]. The newly developed behavioral test protocol appears to be fairly robust, as indicated by similar patterns of learning curves observed in the results from the experiments conducted at the three different laboratories using three strains of mice (C57BL/6, DBA/2 and ICR) and of different ages (from 2 to 8 months old).

4.1. Behavioral indices for acquisition of behavioral sequencing task and behavioral flexibility

4.1.1. Acquisition of behavioral sequencing task

In the behavioral sequencing task, mice were found to rapidly learn place discrimination of rewarded and never-rewarded places with low individual differences. The alternating sequence rule of this task is of importance in accounting for such efficiency. That is, once a mouse received a reward in an "active" rewarded corner, the corner became "inactive", and at the same time, the other diagonally opposite rewarded corner conversely became "active". Thus, mice were obliged to shuttle between the two distantly positioned rewarded corners for additional rewards, avoiding the temptation of entering the neighboring never-rewarded corners. This rule enables to prevent mice from staying a specific corner to get additional rewards without active choice, and thus, to reduce the possibility of misinterpretation of pseudo-learning effect attributed to place preference. Additionally, the behavioral sequencing task concurrently demands cognitive processes for both reinforced alternation and place discrimination. Although this task can be considered to be relatively complex compared with each learning task of reinforced alternation and place discrimination for mice because of its mixed rule, they could acquire this behavioral sequence and show high discriminative performance within the first several sessions. When compared with other established spatial learning paradigms, the learning curves of the discriminative performance in the behavioral sequencing task paradigm were similar to those observed in the Morris water maze [3,53–56] and other maze tasks (e.g., [3,57,58]), despite the differences in experimental designs and indices. Considering the result of the probe trial (see Supplemental Fig. S1 and its legend), we concluded that the behavioral sequencing task paradigm using IntelliCage is an optimized method for the efficient cognitive assessment in mice.

4.1.2. Behavioral flexibility

To date, researchers have tried to establish the mouse as a useful animal model for assessing behavioral inflexibility that is found in human patients with frontal lobe damage, aging-associated cognitive decline, and neuropsychological disorders [29]. The reported methods are based on various approaches such as maze tasks [59,60] and operant conditioning procedures [42,61–65]. However, it is still unclear what types of behavioral measure are suitable for the integrated behavioral flexibility assessment in mice. Thus, the major aim of this study is to characterize a detailed process of behavioral adaptation to the altered action-outcome contingency in mice in a reproducible manner.

A unique feature of the behavioral flexibility assessment in this study is that it can be used to analyze behavioral data in various time scales that span from minutes to even months. In this study, mice were clearly found to develop behavioral flexibility to the altered action-outcome contingency in intra- and inter-session intervals. In the intra-session analysis, we found that mice shifted their preference to the newly assigned rewarded corners within the first sessions of each reversal stage (Rev) (see session 15 in Fig. 5A and B). These indices represent a dynamics of short term behavioral flexibility. In addition, mice showed day-to-day

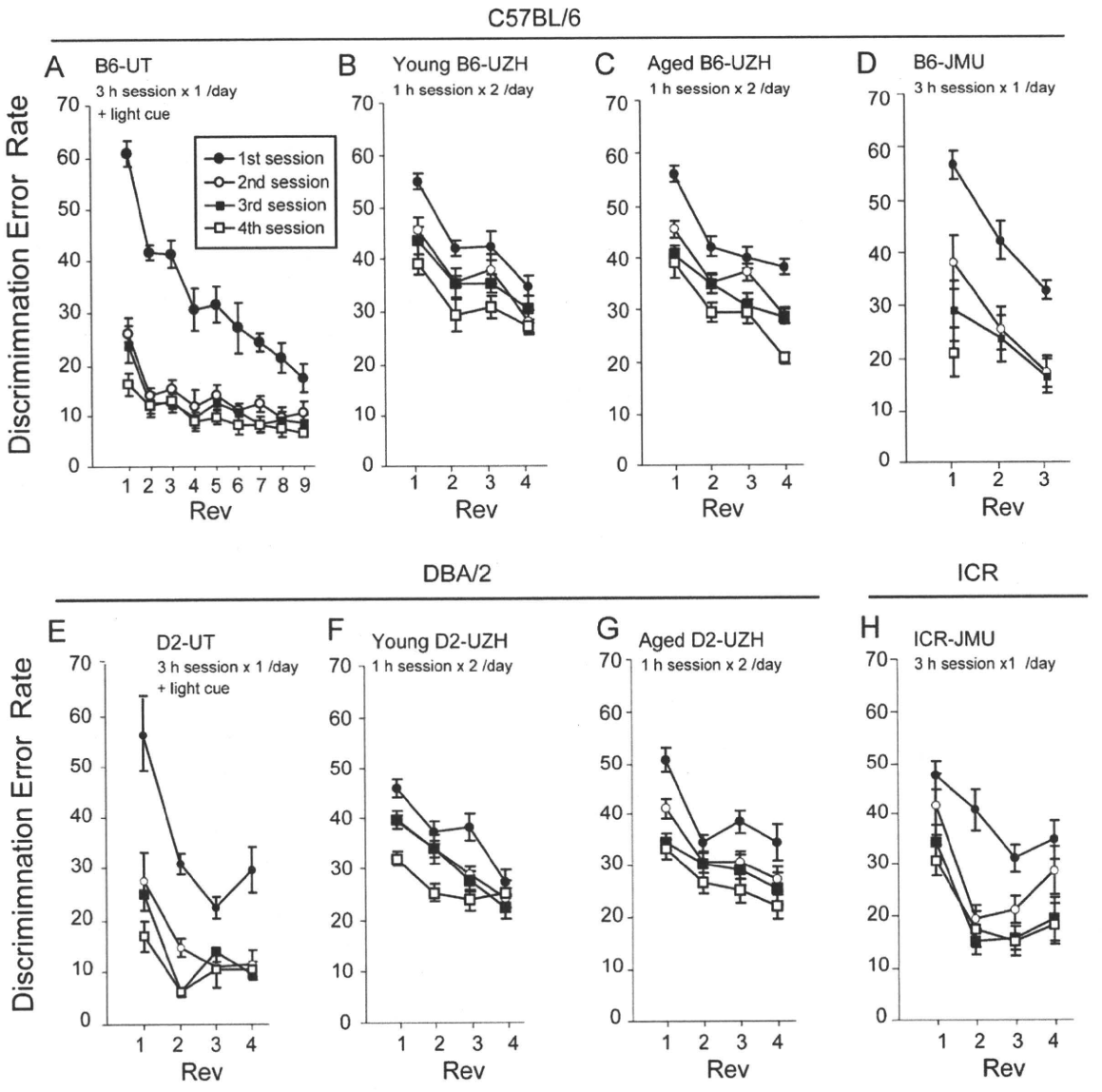

Fig. 6. Long term (inter-reversal stage) improvement of behavioral flexibility in the serial reversal task. (A) B6-UT, (B) Young B6-UZH, (C) Aged B6-UZH, (D) B6-JMU, (E) D2-UT, (F) Young D2-UZH, (G) Aged D2-UZH and (H) ICR-JMU. Panels (A), (B), and (D) were reconstructed using the data shown in Fig. 4. Discrimination error rates of the first, second, third, and fourth sessions from each reversal stage (Rev) were plotted to show the inter-reversal stage (Rev) dynamics of behavioral flexibility (mean ± S.E.M, $n = 8, 11, 12, 15, 8, 12, 11$, and 11, respectively from panel (A) to (H)). The discriminative performance consistently improved among the reversal stages (Revs) in all the eight cohorts from Rev 2 to the subsequent stages, particularly in the first sessions with a significant linear trend of error reduction ($p < 0.05$, repeated measures ANOVA).

improvement of adaptive behavior. In other words, they were found to have inter-session dynamics of behavioral flexibility that forms typical learning curves (Fig. 4). The time course patterns of these learning curves on intra- and inter-sessions were repetitively observed, and thus, considered to be robust in a long term experiment. Therefore, we propose that the present method makes it possible to efficiently characterize the process of behavioral flexibility in mice.

Another feature of the present test is that the reversal learning of the behavioral sequencing task is distinct from other conventional tasks in terms of its behavioral requirements. That is, subjects were required not only to relearn the rewarded locations but also to develop shuttling behavior between the reversed diagonal corners. As in the case of the initial acquisition of the behavioral sequencing task, this paradigm prevents mice from staying at a specific corner to obtain additional rewards without an active choice in reversal learning. As a result, we found that this reversal learning yielded a very clear and consistent form of learning curve in mice. Thus, we concluded that the reversal learning using the behavioral sequencing task established in this study is useful for assessing behavioral flexibility in mice.

4.1.3. Adaptation to "reversal rule"

The serial reversal learning in this study exhibited another intriguing phenomenon, that is, a progressive enhancement in adaptation to reversal learning. In particular, the B6-UT mice, which were the most trained cohort in this study, swiftly shifted to the new spatial pattern in the final phase of the long term flexibility test (see Fig. 7A and Supplemental Fig. S4). The ability of the progressive shifting from trial-and-error to the immediate solving of new problems on the basis of previously learned experiences can be explained using the theory of "learning-set", which indicates that animals can learn to learn (a formation of learning-set). This theory was established by Harry F. Harlow following his pioneering experiments [66] using monkeys that showed errorless solving after a number of discrimination problems, indicating that they had grasped the rule characterizing the task. More specifically, a reversal learning-set is a phenomenon described as a progressive